Dynamic properties of liquid cesium near the melting point: A molecular-dynamics study

Shaw Kambayashi* and Gerhard Kahl
Institut für Theoretische Physik, Technische Universität Wien, Wiedner Haupstrasse, 8-10, A-1040 Wien, Austria
(Received 6 March 1992)

We present results of a molecular-dynamics study on liquid cesium, just above the melting point; i.e., we have performed a *computer* experiment on exactly the same system that was studied recently in a very accurate *neutron-scattering* experiment by Bodensteiner *et al.* In this simulation the interaction of the cesium atoms is based on an Ashcroft empty-core pseudopotential; the total simulation length extends over 100 000 time steps, i.e., 8×10^{-10} s real time. Both static and dynamic structure factors are in very good agreement with experimental results: as in the experiment, we also get—within very good accuracy—a positive dispersion relation. However, concerning propagating sound modes beyond the main peak in $S(q)$ ($q \geq q_p \sim 1.4$ Å) we cannot find sufficient evidence for their existence. Analysis of the transverse current correlation function shows that the corresponding decay mechanism is built up by two relaxation processes (a fast binary one and a slow collective one); starting from ~ 1 Å^{-1} the latter one is completely extinguished. The correlation functions are fitted to hydrodynamic and memory-function models that contain generalized thermodynamic and elastic quantities as parameters. In several cases—if statistics allows—the true physical values can be recovered; then agreement with experimental values is quite satisfactory (differences of 10–15 % are observed).

PACS number(s): 61.20.Ja

I. INTRODUCTION

In a recent series of contributions, Bodensteiner *et al.* [1] presented results of a very detailed and accurate neutron-scattering study of the dynamic properties of liquid cesium just above the melting point (i.e., at a temperature of 308 K and a mass density of 1832.1 kg m^{-3}). *This* contribution reports on investigations on the same system; however, this time the experiment has been performed by a molecular-dynamics (MD) simulation on a *computer.* Preliminary results have already been presented [2].

The first calculations ever done on the dynamic properties of a liquid date back to 1964 (Rahman [3]) which were performed for a Lennard-Jones (LJ) system. Since that time, such systems have been studied thoroughly (starting from the work by Levesque and co-workers [4,5] up to recent contributions by Hoheisel and co-workers [6–8]; for an overview see Boon and Yip [9]). Besides LJ systems, also hard spheres have been studied very carefully (again see Boon and Yip [9]), so that we have now a very detailed picture of the dynamics of these two liquids.

Concerning liquid metals, the situation is different: although the first calculations were already done in 1974 (again by Rahman [10] in a parallel project to neutron-scattering experiments [11]) and although it was already clear around 1980 that liquid metals and LJ systems *do* have a distinctly different dynamic behavior [12,13], our knowledge on the dynamic properties of liquid metals extracted from computer experiments is not so comprehensive as it is in the case for LJ liquids. This is of course partly due to the fact that liquid metal potentials are—in contrast to a LJ potential—explicitly density dependent, therefore—even if we restrict ourselves (as in this study) only to a simple model potential—a large variety of potential forms exists across the Periodic Table [14]. Among the liquid metals investigated recently in computer experiments we find Rb [15,16], Bi, and Pb [17]; this list does not claim to be complete.

During the past few years experimentalists have made much progress in the determination of dynamic properties of liquid metals: better neutron sources, improved algorithms for correcting different errors, etc., guarantee extremely accurate experimental data. If we restrict ourselves to the alkali metals only we now have experimental results for practically all elements of this group (Li [18], Na [19], Rb [20], and Cs [1]); in the case of Li and Na, we even have both coherent and incoherent neutron-scattering results due to the fact that the corresponding cross sections are sufficiently large. This development, in turn, is a challenge for the theorist: improved MD codes (which, e.g., guarantee a very accurate integration of the equations of motion) and improved methods to interpret the raw computer data have been developed [9,21] and applied. Nowadays, high-performance computers allow even the treatment of large systems (e.g., up to 16 000 particles [17]) over an extremely large number of integration steps (100 000–1 000 000).

To check the reliability of our method we have chosen Cs for this study. Extension of our calculations to other liquid metals, especially the other alkali metals, is planned. Our Cs atoms interact via a simple Ashcroft empty-core pseudopotential [22], using the Ichimaru-Utsumi [23] parametrization for the local field correction. Despite its simplicity, this model gives for the static properties good agreement with experimental data [24]. Using a time step Δt of 8×10^{-15} s the simulation was performed over 100 000Δt for different system sizes up to 2048 particles. The positions $\mathbf{r}_i(t)$ and velocities $\mathbf{v}_i(t)$ of the particles are sufficient to construct all the dynamic

 ©1992 The American Physical Society

correlation functions (CF's) presented here: the self-dynamic-structure-factor $S_s(q,\omega)$, the velocity autocorrelation function (VACF) $\Psi(t)$, and the transverse and longitudinal CF's [the latter being closely related to the dynamic structure factor $S(q,\omega)$]. Unfortunately the single particle CF's could not be compared to experimental data, since a too small incoherent neutron-scattering cross section does not allow their determination from experiment. We have compared our $S(q,\omega)$ and the dispersion relation $\omega_l^m(q)$ with the experimental results: we find an astonishingly good agreement; especially, the positivity of the dispersion relation is reproduced with high accuracy. Investigations on the transverse CF (which is not accessible from experiment) confirm in agreement with Jacucci and McDonald [12] that liquid metals are able to support shear waves from very small q's onward (in our case $q \sim 0.0732$ Å^{-1}); furthermore, we find that the relaxation process of the transverse modes is built up from two relaxation processes (a fast binary and a slow collective one), the latter one being completely extinguished from $q \sim 1$ Å^{-1} onward, thus including the position of the main peak in $S(q)$.

The different CF's have been fitted via hydrodynamic and memory-function models, which contain generalized, q-dependent thermodynamic and elastic constants as parameters. In principle the true physical values of these quantities are recovered by extrapolating them towards $q=0$. However, it turns out that not in all cases is such an extrapolation possible due to numerical reasons. If we can recover thermodynamic and elastic constants from our calculations they are in general in good agreement with experiment [25,26] (differences of 10–15 % are observed).

This paper is organized as follows: in Sec. II we have compiled all the details about the theoretical tools necessary for our investigations, i.e., the construction of the potentials and parameters of the MD run. Section III contains the definitions of the dynamic CF's calculated here and related quantities; different methods which interpret those CF's by means of models are presented. Section IV is devoted to the discussion of our results in comparison with the experimental data (static and dynamic CF's as well as thermodynamic and elastic properties). The paper is concluded with a summary.

II. MODEL AND SIMULATION

A. The interatomic potential

The system we have studied is liquid cesium just above the melting point, i.e., at a temperature $T=308$ K and a mass density $n=1832.1$ kg m^{-3} [1,25]; it is exactly the same state which was investigated recently in an experiment by Bodensteiner *et al.* [1].

The cesium atoms interact via an effective two-body potential $\Phi(r)$ which is based on pseudopotential theory. Its Fourier transform (FT) $\hat{\Phi}(q)$ is given by

$$\hat{\Phi}(q)=\frac{4\pi e^2}{q^2}+\frac{4\pi e^2}{q^2}\left[\frac{1}{\epsilon(q)}-1\right]|\hat{v}(q)|^2 , \tag{1}$$

$$\epsilon(q)=1-\frac{4\pi e^2}{q^2}\chi(q)\left[1+\frac{4\pi e^2}{q^2}G(q)\chi(q)\right] . \tag{2}$$

$\chi(q)$ is the usual Lindhard susceptibility function, $G(q)$ is the local field correction, and $\hat{v}(q)$ is the bare local pseudopotential. Among the many approximations proposed in the literature for $G(q)$ (for an overview see Hafner [27]), the parametrization of Ichimaru-Utsumi [23] seems to us to represent the best compromise between accuracy and computational efficiency. For $\hat{v}(q)$ we have chosen a simple Ashcroft empty-core pseudopotential [22], given by

$$\hat{v}(q)=-\frac{4\pi e^2}{q^2}\cos(qr_c) . \tag{3}$$

Although nowadays more sophisticated methods exist to construct effective interatomic potentials in liquids (for an overview see again Hafner [27]), we stick to this rather simple model; this type of interaction has only one parameter (r_c) and it has turned out that such a potential is able to produce excellent results for the static structure (using different liquid-state methods, as computer simulations, perturbation theories and integral equations) not only for the alkali metals, but also for quite a large number of simple metals [28]. In our case r_c is chosen to be 2.72 a.u., a value which is usually accepted in the literature and which is justified by the following criteria: (i) it provides good agreement between theory and experiment for the static structure factor $S(q)$ of liquid Cs over a wide range of temperature [24], (ii) it guarantees a zero-pressure condition for the solid state [27], and (iii) resulting values of the longitudinal and transverse phonon frequencies of the solid state are in good agreement with those obtained by more sophisticated pseudopotential theories (as, e.g., the "generalized pseudopotential theory" [29]) and with experiments [30,31] (cf. Table I). $\Phi(r)$ is depicted in Fig. 1. The potential constructed in this way shows the well-known long-ranged Friedel oscillations which represent a characteristic difference to simple model potentials as the LJ potential. This, in turn, will cause a different dynamic behavior, as will be seen in this contribution.

B. The simulation

The simulation has been performed using a standard microcanonical MD code with the usual periodic bound-

TABLE I. Longitudinal (L) and transverse (T) phonon frequencies for cesium at the Brillouin-zone boundary, calculated from the "generalized pseudopotential theory" (GPT) [29], from this model potential and as obtained from two different experiments [30,31] (all values in ps^{-1}).

Direction	GPT [29]	This potential	Expt. [30]	Expt. [31]
L[100]	1.04	1.080	1.01	0.90
L[110]	1.19	1.080	1.04	1.07
T_1[110]	0.21	0.267	0.22	0.22
T_2[110]	0.68	0.708	0.57	0.58

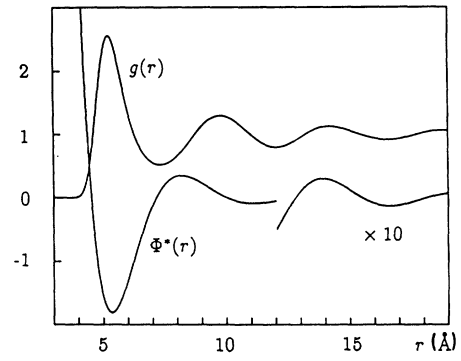

FIG. 1. Pair distribution function $g(r)$ and reduced dimensionless interatomic potential $\Phi^*(r)=\beta\Phi(r)$ for the system investigated as functions of r.

ary conditions; the equations of motion are integrated by means of a fourth-order predictor-corrector Gear algorithm [32]. Keeping the mass density n fixed to the experimental value of 1832.1 kg m^{-3} [1,25], we used four different system sizes, characterized by the particle numbers $N=256$, 500, 1372, and 2048. This was done in order to study size effects both on the dynamic CF's, and on the thermodynamic and elastic properties (cf. Secs. III and IV).

As we shall see in Sec. III, the positions $\mathbf{r}_i(t)$ and the velocities $\mathbf{v}_i(t), i=1,\ldots,N$ provided by the MD for every particle are the only ingredients necessary to construct the different dynamic CF's, which, in turn, allow us to extract thermodynamic and elastic data.

All MD runs were performed over 100 000 time steps, using a time increment Δt of 8×10^{-15} s. In all cases energy conservation for the *whole* MD run was less than 0.01%, due to the value of Δt, the grid size of the tabulated potential (see below) and the sophisticated integration method. Both static and dynamic CF's are obtained by averaging over time, invoking the ergodic hypothesis of the equality of time averaging and ensemble averaging. Temperature and energy were recorded during the whole run, since their time dependence may provide us further information on the system.

The potential was calculated in tabular form on a grid with a mesh size of 0.04 Å. Except for the smallest system, it was truncated at a distance $r_{\rm cut}=18.12$ Å, i.e., after the sixth node, just before the fourth maximum; for the smallest system $r_{\rm cut}$ was chosen to be 12.8 Å, since the sixth node would have been outside the simulation box. $r_{\rm cut}$ corresponds from 42.6% ($N=500$) to 28.9% ($N=2048$) of the side length L_N of the simulation box. This distance seems to us to be sufficient to include all important contributions of the potential: at the position of the fourth maximum (the first extremum *beyond* $r_{\rm cut}$), the potential $\Phi(r)$ has dropped to 0.374% of its value at its first minimum (cf. Fig. 1).

Associated with every dynamic CF is a wave vector $\mathbf{q}$, which in the experiment may be chosen deliberately.

TABLE II. Recurrence time $t_{\rm rec}$ (assuming the experimental value for the velocity of sound of 965 m s^{-1}) as defined in the text; wave numbers q (in Å^{-1}) both for the different system sizes used in the MD simulation and chosen in experiment [1].

256 $t_{\rm rec}=3.25$ ps		500 $t_{\rm rec}=4.06$ ps		1372 $t_{\rm rec}=5.69$ ps		2048 $t_{\rm rec}=6.50$ ps		Expt. [1]
q	N_q	q	N_q	q	N_q	q	N_q	q
0.400 58	3	0.160 23	3	0.114 45	3	0.100 15	3	0.2
0.633 77	12	0.226 60	6	0.161 86	6	0.141 63	6	0.3
0.895 73	12	0.392 49	12	0.198 24	4	0.173 46	4	0.4
1.313 40	12	0.506 70	12	0.228 91	3	0.223 93	12	0.5
2.002 92	15	0.640 93	3	0.396 47	4	0.400 58	3	0.6
2.403 50	15	0.698 44	12	0.498 89	12	0.656 70	12	0.7
2.775 32	4	0.751 56	12	0.594 71	16	1.040 75	16	0.8
3.204 66	3	0.906 42	6	0.647 44	6	1.133 02	6	0.9
3.582 92	12	1.013 40	12	0.750 51	12	1.278 58	12	1.0
4.005 83	15	1.110 13	4	0.915 62	3	1.387 66	4	1.15
		1.281 87	3	1.023 69	12	1.525 37	12	1.2
		1.396 88	12	1.121 40	12			1.25
		1.503 12	12	1.189 42	16			1.3
		1.602 33	15	1.294 88	6			1.4
		1.812 83	6	1.392 37	12			1.5
				1.501 03	12			1.6
				1.585 90	4			1.7
				1.743 29	12			1.8
				1.873 66	12			1.9
				1.995 54	12			2.0
				2.147 32	12			2.2
				2.242 80	12			2.4
				2.378 85	16			2.55
				2.784 74	12			

TABLE III. CPU time per integration step (in s).

N	Time
256	0.025
500	0.091
1372	0.57
2048	1.07

However, as the MD algorithm is restricted to periodic boundary conditions, the wave vectors $\mathbf{q}$ have to satisfy the condition $\mathbf{q}=(2\pi/L_N)(n_1,n_2,n_3)$, where the n_i are integers. Since our system is isotropic, the CF's are functions of $q=|\mathbf{q}|$ only. Given a value of q, N_q vectors $\mathbf{q}$ exist with the same modulus. Since—due to statistics—the results obtained from MD are not completely direction independent (differences up to several percent are observed), the final result of a CF is an average over all N_q directions (as will be explained in Sec. III). Among those $\mathbf{q}$'s, which are compatible with the periodic boundary condition, our choice was according to the following criteria: (i) in order to enable comparison with experiment, they should be near those q values chosen in the experimental study [1]; (ii) to study size effects, several of them were chosen to satisfy $q_N \sim q_{N'}, N \neq N'$ (within an accuracy of 1 or 2%); (iii) due to technical reasons, those q's with N_q larger than 16 were discarded. All q's used in this study for the four different system sizes are compiled together with the corresponding N_q's and the experimental q values in Table II. The respective first values represent—except for $N=256$—the smallest q's compatible with periodic boundary conditions.

All calculations were performed on a VP50-EX vector processor. The CPU times necessary for one integration step for the different system sizes are presented in Table III.

III. THE CORRELATION FUNCTIONS

From the MD run we obtain the positions $\mathbf{r}_i(t)$ and velocities $\mathbf{v}_i(t)$ at times $t=j\Delta t$, $j=1,\ldots,100\,000$. This information is sufficient to construct all the quantities we need: we define the FT of the density operator and current operator,

$$\rho_{\mathbf{q}}(t)=\sum_{i=1}^{N}\exp[-i\mathbf{q}\cdot\mathbf{r}_i(t)]\ ,$$
$$\mathbf{j}_{\mathbf{q}}(t)=\sum_{i=1}^{N}\mathbf{v}_i(t)\exp[-i\mathbf{q}\cdot\mathbf{r}_i(t)]\ , \tag{4}$$

where $\mathbf{q}$ is a vector chosen according to the criteria of Sec. II.

In the following we will introduce four different dynamic CF's. In the theoretical study these functions are obtained as functions of time, while in experiment they are determined as functions of frequency ω; in order to enable a direct comparison with experiment we have to perform a FT. However, a closer analysis of our results leaves us no hope to perform these transformations directly, i.e., without further analysis: neither the experimental nor the theoretical CF's may be determined over a sufficiently large range in ω or t space (i.e., until they have decayed to guarantee a sufficient numerical accuracy). Therefore procedures to fit these functions in t and/or ω space to analytical expressions have become handsome tools to perform these transformations either analytically or numerically with a deliberate degree of accuracy. These expressions are based on different approaches; in this contribution we shall restrict ourselves to the hydrodynamic fit (HF), valid in the low-q–low-ω region and the memory-function (MF) ansatz. In both cases these expressions contain generalized q-dependent thermodynamic and elastic parameters, their true physical values are obtained in the limit $q\to 0$; they therefore might give us a possibility to extract such data from our results and to compare the corresponding theoretical and experimental values. However, we shall see that an extrapolation towards $q=0$ is not always possible due to numerical reasons.

A. Static correlation functions

The pair distribution function (PDF) $g(r)$ is obtained by sampling every 40 time steps. Its FT, obtained via

$$S(q)=1+\rho\int[g(r)-1]e^{-i\mathbf{q}\cdot\mathbf{r}}d\mathbf{r}\ , \tag{5}$$

is the static structure factor. $\rho=n/M$ is the number density and M is the mass of the atoms. The respective positions of the main peaks of these functions will be denoted by $a\,[g(r)]$ and $q_p[S(q)]$.

B. Self-correlation-functions

The self-intermediate-scattering-function $F_s(q,t)$ is defined as

$$F_s(q,t)=\langle e^{i\mathbf{q}\cdot[\mathbf{r}_1(t)-\mathbf{r}_1(0)]}\rangle\ . \tag{6}$$

This definition contains two averages: (i) one is the average over all N_q possible vectors $\mathbf{q}$ with $|\mathbf{q}|=q$, i.e., $F_s(q,t)=(1/N_q)\sum_{\mathbf{q}}F_s(\mathbf{q},t)$; (ii) the symbols $\langle\ \rangle$ denote averaging along the trajectories of the particles (according to Levesque and Ashurst [33]), by shifting origins by $\Delta t_0=1250\Delta t$ and averaging over particles, i.e.,

$$F_s(q,t)=\frac{1}{N}\sum_{i=1}^{N}\left[\sum_{j=1}^{N_T}e^{i\mathbf{q}\cdot[\mathbf{r}_i(t+j\Delta t_0)-\mathbf{r}_i(j\Delta t_0)]}\right]\ . \tag{7}$$

If we denote the time span over which the CF is recorded by t_t and the number of t_t's over which we average by N_T then we have used the following values: $N_T=80$, $t_t=1250\Delta t$. The FT of Eq. (6) is the self-dynamic-structure-factor

$$S_s(q,\omega)=\frac{1}{2\pi}\int_{-\infty}^{\infty}e^{i\omega t}F_s(q,t)dt\ . \tag{8}$$

For a given q, the frequency moments (sum rules) are defined as

$$\omega_s^n(q)=\int_{-\infty}^{\infty}\omega^n S_s(q,\omega)d\omega=(-1)^{n/2}F_s^{(n)}(q,t)|_{t=0}$$

(only the even moments are nonzero). Being static CF's, these moments may be expressed in terms of the PDF and higher-order distribution functions: $g(r)$ may easily

be extracted from the MD run. The distribution function of the next order, i.e., $g^{(3)}(\mathbf{r},\mathbf{r})$, may, in principle also be obtained from simulations: however, this procedure is extremely time-consuming [34,35] and therefore not realistic. And although several attempts have been made to get $g^{(3)}(\mathbf{r},\mathbf{r}')$ from numerical approaches for the whole $(\mathbf{r},\mathbf{r}')$ space (as required for the integrations) [36], they are too time-consuming for practical use. Besides that, the higher moments involve correlations between increasing numbers of particles and rapidly become very tedious to evaluate [21]. We therefore restrict ourselves (and this will also be the case for all the other dynamic CF's which we shall discuss in the following) only to those moments which may be calculated by means of the PDF, i.e., for the case of $F_s(q,t)$ up to the fourth moment:

$$\omega_s^0=1\ ,\quad \omega_s^2=(qv_0)^2\equiv\omega_0^2\ , \tag{9}$$

$$\omega_s^4=3(qv_0)^4+\omega_0^2\frac{\rho}{M}\int d\mathbf{r}\,g(r)\frac{\partial^2 u}{\partial z^2}\equiv 3(qv_0)^4+\omega_0^2\Omega_0^2\ . \tag{10}$$

The above equations may be considered as definitions of ω_0^2 and the Einstein frequency $\Omega_0^2;v_0^2=1/\beta M$ is the thermal speed.

We now present two different expressions which enable us to fit our data and to perform then the FT (8) analytically and/or numerically (within sufficient numerical accuracy): (i) the HF expression is valid in the hydrodynamic region, i.e., for small q's and small ω's,

$$F_s(q,t)=e^{-Dq^2t},\quad S_s(q,\omega)=\frac{1}{\pi}\frac{Dq^2}{(Dq^2)^2+\omega^2}\ , \tag{11}$$

where D is the diffusion constant.

(ii) In the MF formalism the CF's [here $F_s(q,t)$] and its MF [$M_s(q,t)$] fulfill the following relation:

$$\frac{\partial}{\partial t}F_s(q,t)+\int_0^t M_s(q,t-t')F_s(q,t')dt'=0\ . \tag{12}$$

The value $M_s(q,t)|_{t=0}$ is fixed by the condition

$$M_s(q,t)|_{t=0}=-\ddot{F}_s(q,t)|_{t=0}/F_s(q,t)|_{t=0}=\omega_s^2/\omega_s^0\ . \tag{13}$$

Continuing this scheme we can make a MF ansatz for $M_s(q,t)$[its MF is $N_s(q,t)$], $N_s(q,t)|_{t=0}$ being fixed by

$$N_s(q,t)|_{t=0}=-\frac{\dddot{M}_s(q,t)|_{t=0}}{M_s(q,t)|_{t=0}}=\frac{F_s^{(4)}(q,t)|_{t=0}}{\ddot{F}_s(q,t)|_{t=0}}-\frac{\ddot{F}_s(q,t)|_{t=0}}{F_s(q,t)|_{t=0}}=\frac{\omega_s^4}{\omega_s^2}-\frac{\omega_s^2}{\omega_s^0}\ . \tag{14}$$

Truncating this procedure (which guarantees the sum rules up to fourth order) we obtain for the Fourier-Laplace-transform $\tilde{F}_s(q,\omega)[=\int_0^\infty \exp(i\omega t)F_s(q,t)dt]$ of the self-intermediate-scattering-function

$$\tilde{F}_s(q,\omega)=\frac{1}{-i\omega+\dfrac{\omega_s^2}{-i\omega+\tilde{N}_s(q,\omega)}}\ . \tag{15}$$

For N_s we make the following simple (exponential) ansatz:

$$\tilde{N}_s(q,\omega)=(2\omega_0^2+\Omega_0^2)\tilde{n}_s(q,\omega)\ ,\quad n_s(q,t)=e^{-t/\tau_s}\ ,\quad n_s(q,t)|_{t=0}=1\ , \tag{16}$$

and we obtain, for

$$S_s(q,\omega)=\frac{1}{\pi}\mathrm{Re}[\tilde{F}_s(q,\omega)]\ ,$$

$$S_s(q,\omega)=\frac{1}{\pi}\frac{\tau_s\omega_0^2(2\omega_0^2+\Omega_0^2)}{\tau_s^2\omega^2(3\omega_0^2+\Omega_0^2-\omega^2)^2+(\omega_0^2-\omega^2)^2}\ , \tag{17}$$

where the limit

$$\lim_{q\to 0}\tau_s(q)=\frac{v_0^2}{D\Omega_0^2} \tag{18}$$

is consistent with the hydrodynamic limit (11).

The normalized VACF is defined as

$$\psi(t)=\frac{\langle \mathbf{v}_1(t)\cdot\mathbf{v}_1(0)\rangle}{\langle \mathbf{v}_1(0)\cdot\mathbf{v}_1(0)\rangle}=\frac{1}{3v_0^2}\langle \mathbf{v}_1(t)\cdot\mathbf{v}_1(0)\rangle\ , \tag{19}$$

where averaging $\langle\ \rangle$ is done in the same way as in (7) with the same parameters Δt_0, N_T, and t_t. We define the Fourier spectrum $\Psi(\omega)$ and the moments ω_v^n

$$\Psi(\omega)=\frac{1}{2\pi}\int_{-\infty}^{\infty}e^{i\omega t}\Psi(t)dt\ , \tag{20}$$

$$\omega_v^n=\int_{-\infty}^{\infty}\omega^n\Psi(\omega)d\omega,\quad \omega_v^0=1,\quad \omega_v^2=\Omega_0^2 \tag{21}$$

The first-order MF ansatz for $\tilde{\Psi}(\omega)$

$$\tilde{\Psi}(\omega)=\frac{1}{-i\omega+\tilde{M}_v(\omega)} \tag{22}$$

with $\tilde{M}_v(\omega)=\omega_v^2\tilde{m}_v(\omega)$, $m_v(t)|_{t=0}=1$, and $m_v(t)=\exp(-t/\tau_v)$ yields

$$\Psi(\omega)=\frac{1}{\pi}\frac{\omega_v^2}{\tau_v}\frac{1}{(\omega_v^2-\omega^2)^2+\omega^2/\tau_v^2}\ , \tag{23}$$

$$\Psi(t)=\begin{cases}e^{-\frac{1}{2}(t/\tau_v)}\left[\cos(\Omega_1 t)+\dfrac{1}{2\Omega_1\tau_v}\sin(\Omega_1 t)\right], & \Omega_0\tau_v>\frac{1}{2}\\ \dfrac{1}{\omega_+-\omega_-}[\omega_+e^{-\omega_- t}-\omega_-e^{-\omega_+ t}], & \Omega_0\tau_v<\frac{1}{2}\end{cases} \tag{24}$$

(25)

where $\Omega_1^2=\Omega_0^2-\dfrac{1}{4\tau_v^2}$, $\omega_\pm=\dfrac{1}{2\tau_v}[1\mp(1-4\Omega_0^2\tau_v^2)^{1/2}]$.

From the equation [9,21]

$$D=v_0^2\int_0^\infty\Psi(t)dt \tag{26}$$

we obtain a relation between D and τ_v, namely $\tau_v=v_0^2/(D\Omega_0^2)$.

$F_s(q,t)$ may be written in the following form (cumulant expansion [9]):

$$F_s(q,t)=e^{-q^2\rho_1(t)+q^4\rho_2(t)-\cdots}\ . \tag{27}$$

The $\rho_n(t)$ are time-dependent functions which can be calculated from the spatial moments. Neglecting all terms beyond the first one in the exponent of (27) we obtain the so-called Gaussian approximation. Within this approximation a relation between $F_s(q,t)$ and $\Psi(t)$ is given as

$$F_s(q,t)=\exp[-q^2\rho_1(t)],\quad \Psi(t)=\frac{1}{v_0^2}\ddot{\rho}_1(t)\ . \tag{28}$$

C. Dynamic structure factor, current correlation functions

The intermediate scattering function $F(q,t)$ and the current CF's $C_{\alpha\beta}(q,t)$ are defined as

$$F(q,t)=\frac{1}{N}\langle\rho_{\mathbf{q}}(t)\rho_{-\mathbf{q}}(0)\rangle\ , \tag{29}$$

$$C_{\alpha\beta}(q,t)=\frac{q^2}{N}\langle j^{\alpha}_{\mathbf{q}}(t)j^{\beta}_{-\mathbf{q}}(0)\rangle$$
$$=\frac{q_\alpha q_\beta}{q^2}C_l(q,t)+\left[\delta_{\alpha\beta}-\frac{q_\alpha q_\beta}{q^2}C_t(q,t)\right]\ , \tag{30}$$

where $\langle\ \rangle$ does not include averaging over particles [i.e., the inner average of (7) only]. The current CF's are split up into longitudinal (l) and transverse (t) components (the greek indices denote Cartesian coordinates). We choose the following parameters: $\Delta t_0=4\Delta t$, $\Delta t_t=1024\Delta t$, and $N_T=25\,000$, so that the averaging events overlap in contrast to $F_s(q,t)$ and $\Psi(t)$.

The respective FT's and moments are defined as

$$S(q,\omega)=\frac{1}{2\pi}\int_{-\infty}^{\infty}e^{i\omega t}F(q,t)dt,$$
$$C_{l\ (t)}(q,\omega)=\frac{1}{2\pi}\int_{-\infty}^{\infty}e^{i\omega t}C_{l\ (t)}(q,t)dt\ , \tag{31}$$

$$\omega_0^n(q)=\int_{-\infty}^{\infty}\omega^n S(q,\omega)d\omega,$$
$$\omega_{l\ (t)}^n(q)=\int_{-\infty}^{\infty}\omega^n C_{l\ (t)}(q,\omega)d\omega\ . \tag{32}$$

The following important relations hold:

$$C_l(q,\omega)=\omega^2 S(q,\omega),\quad \omega_0^n=\omega_l^{n-2}\ . \tag{33}$$

The dynamic structure factor $S(q,\omega)$ and the self-dynamic-structure-factor $S_s(q,\omega)$ (8) may be compared directly to the experimental results of coherent and incoherent neutron-scattering experiments, as shall be done in Sec. IV.

The sum rules $\omega_0^n(\omega_{l\ (t)}^n)$ up to fourth (second) order are

$$\omega_0^0=S(q),\quad \omega_{l\ (t)}^0=\omega_0^2\ , \tag{34}$$

$$\omega_l^2=3(qv_0)^4+\frac{\rho(qv_0)^2}{M}\int d\mathbf{r}\,g(r)[1-\cos(qz)]\frac{\partial^2 u}{\partial z^2}$$
$$\equiv\frac{q^4v_0^2}{\rho M}[\tfrac{4}{3}G_\infty(q)+K_\infty(q)]\ , \tag{35}$$

$$\omega_t^2=(qv_0)^4+\frac{\rho(qv_0)^2}{M}\int d\mathbf{r}\,g(r)[1-\cos(qz)]\frac{\partial^2 u}{\partial x^2}$$
$$\equiv\frac{q^4v_0^2}{\rho M}G_\infty(q)\ . \tag{36}$$

Here, $G_\infty(q)$ is the wave-number-dependent high-frequency shear modulus, and $K_\infty(q)$ the wave-number-dependent high-frequency bulk modulus.

Due to the factor ω^2 in (33), $C_l(q,\omega)$ shows—in contrast to $S(q,\omega)$—a well-defined peak at a position which shall be denoted as $\omega_l^m(q)$ ($\omega>0$, for *any* q); $\omega_l^m(q)$ is the dispersion relation, the quantity $c_l=\omega_l^m(q)/q$ is the phase velocity of the propagating collective modes. In a similar manner we shall denote—if this peak may be resolved—the position of the ($\omega>0$) peak in $S(q,\omega)$ by $\omega_B(q)$ and the corresponding velocity by $c_B=\omega_B(q)/q$. $\omega_t^m(q)$ defines the position of the ($\omega>0$) peak of $C_t(q,\omega)$, i.e., the dispersion relation of the transverse modes. A phase velocity c_t analogous to c_l will be defined in Sec. IV B.

The FT(31) has been performed in two different ways: (i) first we calculate $S(q,\omega)$ via [37]

$$S(q,\omega)=\frac{1}{2\pi N}\lim_{T\to\infty}\frac{1}{T}\left|\int_0^T\exp(i\omega t)\rho_q(t)dt\right|^2\ , \tag{37}$$

which is equivalent to (31). In order to eliminate the noise caused by the finite trajectories, the result obtained was convoluted with a Gaussian resolution function $f(\omega,\omega_f)$. The parameter ω_f, the full width of these functions, was chosen to guarantee consistency for ω_0^2 (the consistency of ω_0^0 is maintained by definition). ω_f typically ranges from 0.2 to 1 ps^{-1}; (ii) the second possibility for a numerical FT is to fit $F(q,t)$ to different analytical models [HF, MF, as done for $S_s(q,\omega)$ and $\Psi(\omega)$] and to transform these expressions analytically or numerically: for these integrations we can now extend the integrand much further than the original data from the MD run.

In the HF model we find

$$\frac{F(q,t)}{F(q,0)}=\frac{\gamma-1}{\gamma}e^{-D_Tq^2t}+\frac{1}{\gamma}e^{-\Gamma q^2t}[\cos(c_sqt)+b(q)\sin(c_sqt)]\ , \tag{38}$$

$$C_t(q,t)=\omega_t^0e^{-\nu q^2t}\ , \tag{39}$$

$$\frac{S(q,\omega)}{S(q)}=\frac{1}{\pi}\frac{\gamma-1}{\gamma}\frac{D_Tq^2}{\omega^2+(D_Tq^2)^2}+\frac{1}{2\pi\gamma}\left[\left[\frac{\Gamma q^2}{(\omega+c_sq)^2+(\Gamma q^2)^2}+\frac{\Gamma q^2}{(\omega-c_sq)^2+(\Gamma q^2)^2}\right]\right.$$
$$\left.+b(q)\left[\frac{\omega+c_sq}{(\omega+c_sq)^2+(\Gamma q^2)^2}-\frac{\omega-c_sq}{(\omega-c_sq)^2+(\Gamma q^2)^2}\right]\right]\ , \tag{40}$$

$$C_t(q,\omega)=\frac{\omega_t^0}{\pi}\frac{q^2\nu}{(q^2\nu)^2+\omega^2}\ . \tag{41}$$

For a derivation of (38) and (39) see Boon and Yip [9], Hansen and McDonald [21], and Schoen, Vogelsang, and Hoheisel [8]. The FT's with respect to t may be calculated analytically.

The quantities used in the above expressions are the following: c_s is the adiabatic velocity of sound, $\gamma = C_p/C_v$ is the ratio of the specific heats, Γ is the sound attenuation coefficient (which multiplied by q^2 is inversely proportional to the lifetime of the acoustic modes), and D_T is the thermal diffusivity; $b(q) = (q/c_s)[\Gamma + (\gamma - 1)D_T]$ and the kinetic shear viscosity ν is related to the shear viscosity η via $\rho M \nu = \eta$. Γ, D_T and the longitudinal viscosity $\eta_l = \frac{4}{3}\eta + \eta_B$ (η_B is the bulk viscosity) are related via [21]

$$\Gamma = \frac{1}{2}\left[D_T(\gamma - 1) + \frac{\eta_l}{\rho M} \right] . \tag{42}$$

$F(q,t)$ and $C_t(q,t)$ are obtained directly from MD and have been fitted in the hydrodynamic region ($q \leq 0.4$ Å) to the above expressions, using a standard least-square fit procedure, where the parameters c_s, γ, Γ, D_T, and ν are now functions of q. The real physical values are recovered by extrapolating them towards $q = 0$ (cf. Sec. IV C).

Although (38) and (39) are valid only in the hydrodynamic region, we have used (38) to fit $F(q,t)$ for larger q's, since the functional form of this expression seems to be well suited for fitting our MD data. In these cases the obtained parameters lose their physical relevance (they differ too much from their physical values): we simply use this function as a suitable tool to perform a numerically accurate FT (in fact, we have stopped this procedure when for the first time one of the parameters lost physical significance by becoming negative).

We have used for the first-order MF ansatz for $C_l(q,\omega)$ the following, which guarantees consistency of the sum rules ω_l^n up to the second moment:

$$\tilde{C}_l(q,\omega) = \frac{\omega_l^2}{-i\omega + M_l(q,\omega)} , \tag{43}$$

with $M_l(q,t)|_{t=0} = \omega_l^2/\omega_l^0$. The hydrodynamic limit (40) for $S(q,\omega)$ and relation (33) suggest the following expression for $M_l(q,t)$ (a phenomenological derivation is given in Boon and Yip [9], p. 298):

$$M_l(q,t) = \frac{\omega_0^2}{S(q)} + D(q,t), \quad D(q,t) = \frac{\omega_0^2}{S(q)}(\gamma - 1)e^{-D_T q^2 t} + \left[\frac{\omega_l^2}{\omega_0^2} - \gamma \frac{\omega_0^2}{S(q)} \right] m_l(q,t) \tag{44}$$

and $m_l(q,t)|_{t=0} = 1$. Inserting (44) into (43) we obtain

$$C_l(q,\omega) = \omega_0^2 \frac{\omega^2 D'(q,\omega)}{[\omega^2 - \omega_0^2/S(q) + \omega D''(q,\omega)]^2 + [D'(q,\omega)\omega]^2} , \tag{45}$$

where D' and D'' are the real and imaginary part of $D(q,\omega)$. The corresponding $S(q,\omega)$ satisfies the sum rules ω_0^n up to fourth order [21]. Assuming

$$m_l(q,t) = \exp(-t/\tau_l) \tag{46}$$

we have three q-dependent parameters D_T, γ, and τ_l (MF-3); furthermore a one-parameter model (MF-1; parameter: τ_l) is easily obtained from (46) and (44) by fixing γ to unity.

The correct hydrodynamic behavior is guaranteed if

$$n(0) = \frac{\eta_l}{\frac{4}{3}G_\infty(0) + K_\infty(0) - \chi_s^{-1}} , \tag{47}$$

where $\chi_s = (\beta/\rho\gamma)S(0)$ is the adiabatic compressibility.

A MF ansatz for $C_t(q,\omega)$ similar to (43) with $M_t(q,t) = (\omega_t^2/\omega_t^0)m_t(q,t) = [q^2 G_\infty(q)/\rho M]\tilde{m}_t(q,\omega)$ and $m_t(q,t)|_{t=0} = 1$ yields

$$C_t(q,\omega) = \frac{1}{\pi} \frac{\omega_t^2 m_t'(q,\omega)}{\left[\frac{\omega_t^2}{\omega_t^0} m_t''(q,\omega) - \omega \right]^2 + \left[\frac{\omega_t^2}{\omega_t^0} m_t'(q,\omega) \right]^2} . \tag{48}$$

m_t' and m_t'' are the real and imaginary part of $m_t(q,\omega)$. We use two different models for $m_t(q,t)$:

$$\begin{aligned} m_t(q,t) &= \exp(-t/\tau_t) , \\ m_t(q,t) &= [1 - \alpha_t(q)]\exp[-t/\tau_{1t}(q)] \\ &\quad + \alpha_t(q)\exp[-t/\tau_{2t}(q)] . \end{aligned} \tag{49}$$

The correct hydrodynamic behavior (41) is guaranteed if

$$\begin{aligned} \eta &= G_\infty(0)\tau_t(0) , \\ \eta &= G_\infty(0)\{[(1 - \alpha_t(0)]\tau_{1t}(0) + \alpha_t(0)\tau_{2t}(0)\} . \end{aligned} \tag{50}$$

D. Miscellaneous

The static structure factor $S(q)$ has been determined both from the pair distribution function $g(r)$ via (5) as well as from the sum rule (34).

From the temperature fluctuations recorded during the run we can determine the specific heat C_v via

$$\frac{\langle T^2 \rangle - \langle T \rangle^2}{\langle T \rangle^2} = \frac{2}{3N}\left[1 - \frac{3Nk_B}{2C_v} \right] . \tag{51}$$

The diffusion constant D is also accessible via the mean-square displacement:

$$D = \lim_{t \to \infty} \frac{1}{6t} \langle |r(t) - r(0)|^2 \rangle . \tag{52}$$

IV. RESULTS

A. Static structure

Figure 1 shows—together with the potential $\Phi(r)$—the PDF $g(r)$ as obtained from the MD run. The curves for $g(r)$ for different system sizes all coincide within line thickness. Figure 2 shows the static structure factor $S(q)$ as obtained from different theoretical methods [(i) by FT or $g(r)$, (ii) using the sum rule (34)] and in comparison with experimental data [1]; in both cases agreement is very satisfactory. $g(r)$ has furthermore been used to calculate the different moments [cf. (10), (34), (35), (36)]. These integrals have been truncated at the respective r_{cut}'s (cf. Sec. II B). The moments are depicted in Fig. 3. $\omega_l^2(q)$ shows the well-known de Gennes narrowing [38] at the position of the main peak of $S(q)$ ($q_p \sim 1.4$ Å^{-1}); the size dependence of the moments is negligible.

B. Dynamic correlation functions

1. Self-correlation-functions

Both the self-dynamic-structure-factor $S_s(q,\omega)$ and the VACF $\Psi(t)$ have been calculated over a time range of 1250 $\Delta t = 10$ ps for the $N = 2048$ ensemble. Although the time range exceeds the so-called recurrence time (τ_{rec}) for this system size of 6.5 ps (i.e., the time the sound needs for passing through the simulation cell; cf. Table II), this does not seem to affect the CF's. Neither did we find in any paper evidence of effects which might *uniquely* be related to evaluating CF's beyond the recurrence time. We have made closer investigations on this assumption by calculating $\Psi(t)$ for the smaller systems over the same time range. We find that even if we calculate, e.g., $\Psi^{256}(t)$ beyond τ_{rec}^{256}, that this function agrees (within numerical accuracy) with $\Psi^{500}(t)$ in the t range $[\tau_{\text{rec}}^{256}, \tau_{\text{rec}}^{500}]$; this comparison was done for all four system sizes. Since no effects were visible, we may conclude that calculation of CF's beyond τ_{rec} does not have any influence on these functions. The self-intermediate-scattering-function $F_s(q,t)$ is displayed in Fig. 4 for the 11 q-vectors in the $N = 2048$ case. The decay of this function with time is—especially for the smallest q's—very slow, which makes a direct evaluation of $S_s(q,\omega)$ via (8) impossible. We have therefore fitted the computer data both to the HF model (11) and the MF model (17); the latter gives a better quality of fitting than the former. The q-dependence of the respective parameters $D(q)$ and $\tau_s(q)$ is depicted in Fig. 5. While fitting to the HF model is straightforward, the use of the MF expression of $F_s(q,t)$ is a much more delicate task, especially for the smallest q-vectors, where $F_s(q,t)$ is nearly a constant with respect to t; consequently $S_s(q,\omega)$ is a very sharp function of ω. The numerical FT of the analytic $S_s(q,\omega)$ (17) into t space [say $F_s^{\text{HF}}(q,t_i)$, evaluated at discrete times t_i] has been performed using a variable grid size in ω space with

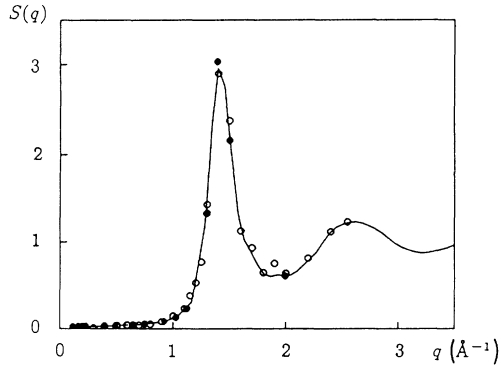

FIG. 2. Static structure factor $S(q)$ for the system investigated. Full line, $S(q)$ as determined from the MD study ($N = 1372$); ○, experimental data [1]; ●, $S(q)$ obtained from the sum rule (34).

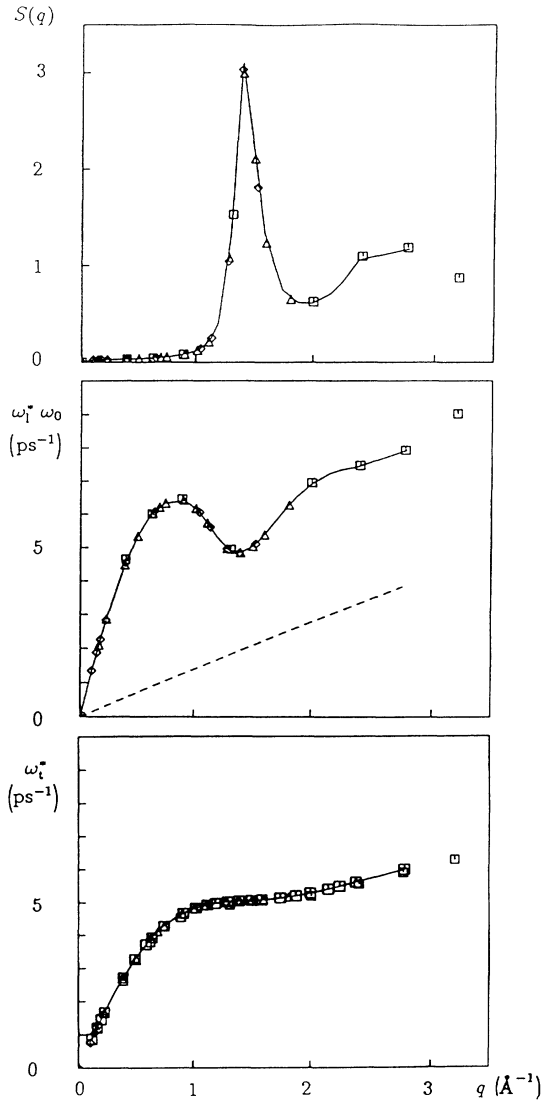

FIG. 3. Wave-number-dependent sum rules for the system investigated as functions of q. Symbols: full line, results for $N = 1372$ (interpolated); □, $N = 256$; △, $N = 500$; ◇, $N = 2048$; (a) $\omega_0^0 = S(q)$, (b) $\omega_l^* = \sqrt{\omega_l^2/\omega_0^2}$, (c) $\omega_t^* = \sqrt{\omega_t^2/\omega_0^2}$. $\omega_0 = qv_0$ is indicated in (b) as a broken line.

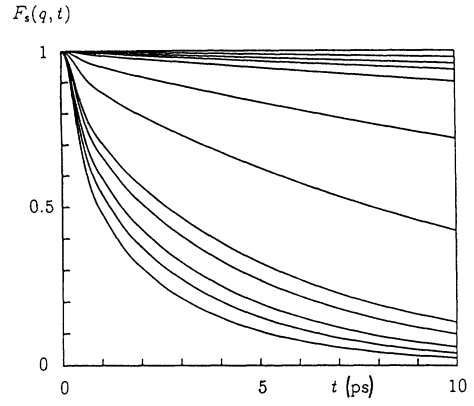

FIG. 4. Self-dynamic-intermediate-scattering-function $F_s(q,t)$ for the system investigated ($N=2048$ ensemble). The q values range from $q=0.100\,15$ Å^{-1} (top) to $q=1.525\,37$ Å^{-1} (bottom). The values of the other q's may be seen from the respective column of Table II.

$2^{14}=16\,384$ points. The sum of the least squares ($\mathcal{S}_s=\sum_{i=1}^{625}[F_s(q,t_i)-F_s^{\mathrm{HF}}(q,t_i)]^2$) is for small q's (up to ~ 0.6 Å^{-1}) typically 0.05; it increases for the largest q values encountered up to 0.5.

Based on this model we have then determined the full width at half maximum $\omega_s^{1/2}(q)$ and the value of $S_s(q,0)$, for which mode-coupling theory (MC) predicts the following behavior for small q's [39]:

$$\omega_s^{1/2}(q)\sim Dq^2(1-aq),\quad S_s(q,0)\sim\frac{1}{\pi D}\frac{1}{q^2}(1+bq)\ . \tag{53}$$

a and b are constants containing the diffusion constant D and the kinetic shear viscosity ν. Both relations are nicely reproduced in our results but will be discussed elsewhere [40], together with a comprehensive discussion of MC effects found in our results. Due to the fact that for Cs the cross section for incoherent neutron scattering amounts to only 10% of the coherent one, we do not have experimental results for $S_s(q,\omega)$. Both $D(q)$ and $\tau_s(q)$ are rather smooth curves for small q's, so that the limit $q\to 0$ may be performed in a numerically safe way; the corresponding values for D will be compared with other values obtained by different methods in Sec. IV C and Table VII.

The VACF $\Psi(t)$ and its Fourier spectrum $\Psi(\omega)$ are displayed in Fig. 6; the latter one could be calculated—due to its rapid decay in time—directly from the simulation data via (20). $\Psi(t)$ has been fitted to the first-order MF model (24), (25) with a rather poor agreement; it therefore is not surprising that we obtain for the diffusion constant D calculated via the fitting parameter τ_v a value which deviates by $\sim 50\%$ from the experimental result (cf. discussion in Sec. IV C and Table VI). But also a different choice for τ_v (using the same MF model)—i.e.,

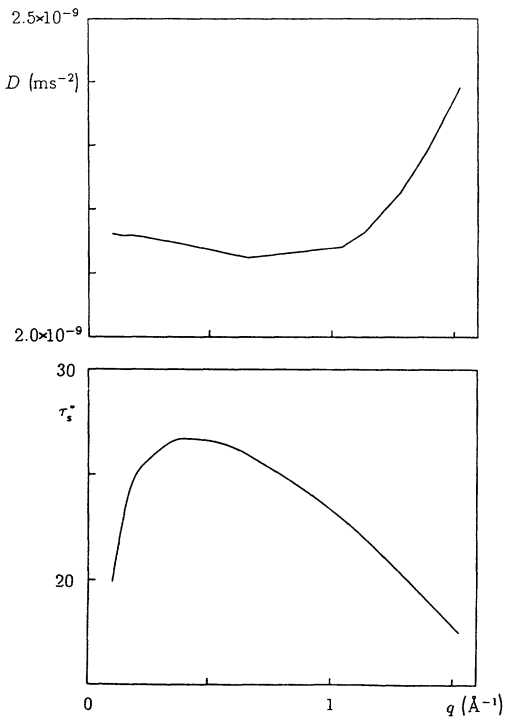

FIG. 5. Generalized diffusion constant $D(q)$ (11) and relaxation time $\tau_s^*(q)=\tau_s/\Delta t$ (17) as obtained from a HF (D), and a MF (τ_s) fit of $S_s(q,\omega)$; $\Delta t=8\times 10^{-15}$ s.

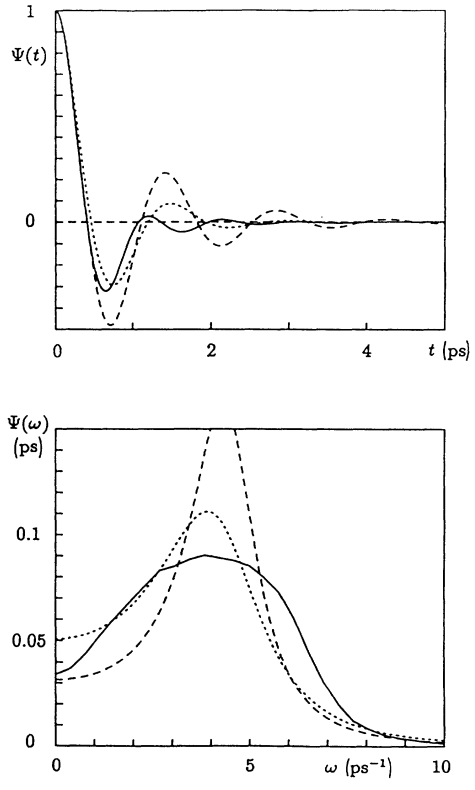

FIG. 6. VACF $\Psi(t)$ (top) and its Fourier spectrum $\Psi(\omega)$ (bottom) of the system investigated ($N=2048$) (full line). The dotted line is the MF fit to $\Psi(t)$ (24), the broken line depicts the MF model, using a $\tau_v=v_0^2/D\Omega_0^2$, where D is obtained via (26).

$\tau_v = v_0^2/D\Omega_0^2$ where D is obtained from time integration of $\Psi(t)$ (26)— does not improve the agreement: again the results are rather poor, so that we may conclude that *in general* this MF model for the VACF is not adequate; an exact *second*-order MF ansatz is, however, not possible due to the lack of knowledge of ω_v^4.

$\Psi(t)$ shows a strong oscillating behavior, which means that the so-called "cage effect" is dominant: due to the rather high density of the system the particles collide very often in quite small cages formed by the other particles and hence quickly lose their memory of their initial velocity. Therefore, a behavior of $\Psi(t) \sim t^{-3/2}$ as observed for hard spheres [41] and in repulsive Lennard-Jones systems [33] and explained by MC theory [42] could not be observed. Such a decay will probably be found at higher temperatures and lower densities where the particles can move more freely and can therefore keep memory of their initial velocity over larger times.

The internal consistency between $F_s(q,t)$ and $\Psi(t)$ has been checked using the Gaussian model. In Lennard-Jones systems this model is found to work well [43]. Figure 7 displays $\Psi(t)$, as obtained both from the computer data and from (28); agreement is very good: this suggests—but of course does not prove—that also here higher-order contributions might be small or even negligible and would correct the Gaussian model only marginally. The function $\rho_1(t)$ itself is depicted in the same figure: both the limit for small t's [where a quadratic behavior $\rho_1(t) \sim v_0^2 t^2/2$ is predicted [9]] as well as the linear long-time behavior $\rho_1(t) \sim Dt$ are very well reproduced.

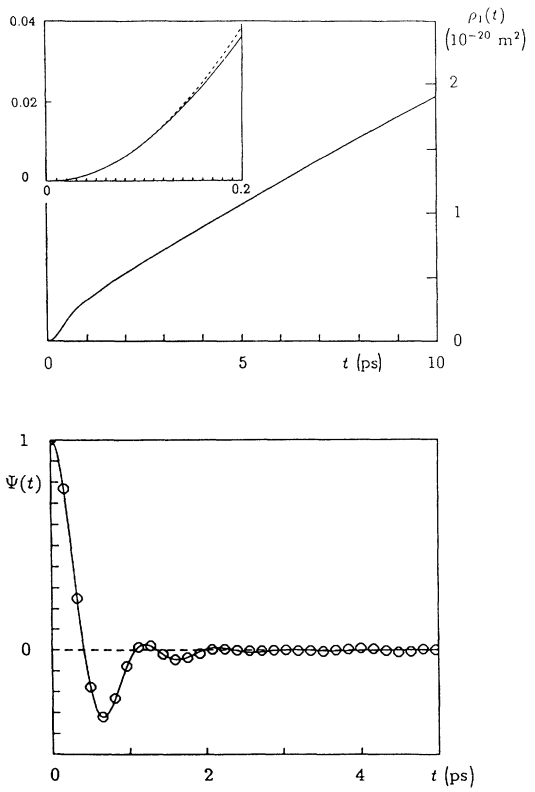

FIG. 7. Gaussian function $\rho_1(t)$ as defined in (28) as a function of time. The inset shows $\rho_1(t)$ in the small-t approximation (dotted line) $\rho_1(t) \sim \frac{1}{2}(v_0 t)^2$ (top). VACF $\Psi(t)$ (bottom) as calculated directly from MD run (line) and as obtained from the Gaussian approximation of $S_s(q,\omega)$ via (28) (symbols) (bottom).

2. *Dynamic structure factor, current correlation functions*

The intermediate scattering function $F(q,t)$ and the transverse current CF $C_t(q,t)$ have been evaluated over $1024\Delta t \sim 8.2\text{ps}(\Delta t = 8\times 10^{-15}$ s), averaging by shifted origins of $\Delta t_0 = 4\Delta t$. Size effects of $F(q,t)$ have been studied by picking up approximately the same q values for the four different system sizes. As may be seen from Fig. 8, the differences are—especially for the larger systems ($N \geq 500$)—not too drastic and should not affect further results too much.

The normalized intermediate scattering function $F_N(q,t) = F(q,t)/F(q,0)$ is depicted in Fig. 9 over the whole q range investigated. While $F(q,t)$ is a strongly oscillating function in t for small q's, the behavior changes drastically at about 1.2 Å^{-1} [which corresponds to the onset of the main peak in $S(q)$; cf. Fig. 2]: $F(q,t)$ becomes a monotonically decreasing function in t; the half width of this line shape has a maximum at q_p and then decreases rapidly. Similar observations have been made and interpreted by Balucani and Vallauri [15] in ordinary and supercooled Rb (see below). For the largest q's investigated, $F(q,t)$ has a needlelike shape. For q values between 1.74 and 2 Å^{-1} a small shoulder is visible; however, this might also be a numerical effect.

The FT from $F(q,t)$ to $S(q,\omega)$ has been performed in three different ways [(i) evaluation of (37), (ii) from HF

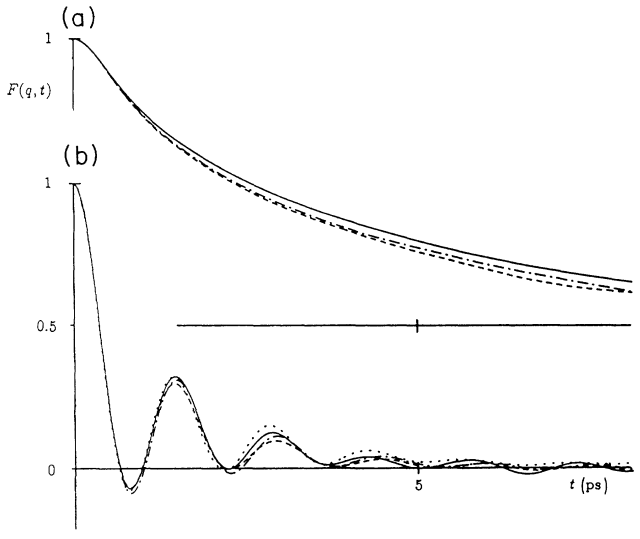

FIG. 8. Size dependence of the normalized intermediate scattering function $F_N(q,t) = F(q,t)/F(q,0)$ for two different q values: (a) $q \sim 0.4$ Å^{-1}, (b) $q \sim 1.5$ Å^{-1}. The q values for different system sizes vary within at most 2% (cf. Table II). Symbols: full line, $N = 1372$; dashed line, $N = 2048$; dashed-dotted line, $N = 500$; and dotted line, $N = 256$.

(40) or (iii) MF fitting (45), (33)]; the results of the different methods are compared in Fig. 10 for several q values; except for the MF-1 results, the procedures can be regarded as equivalent. $\mathcal{S}_0$ (defined in a similar way as $\mathcal{S}_s$ above) reaches—in rare cases—up to 0.1; in general it is less than 0.05. For the sake of completeness we have also depicted the MF-1 curve, which gives for small q's very bad agreement with the other methods, but is of reasonable accuracy for $q \sim 1.2$ Å^{-1} and larger. This reflects the inadequacy of a *one*-relaxation time MF model for

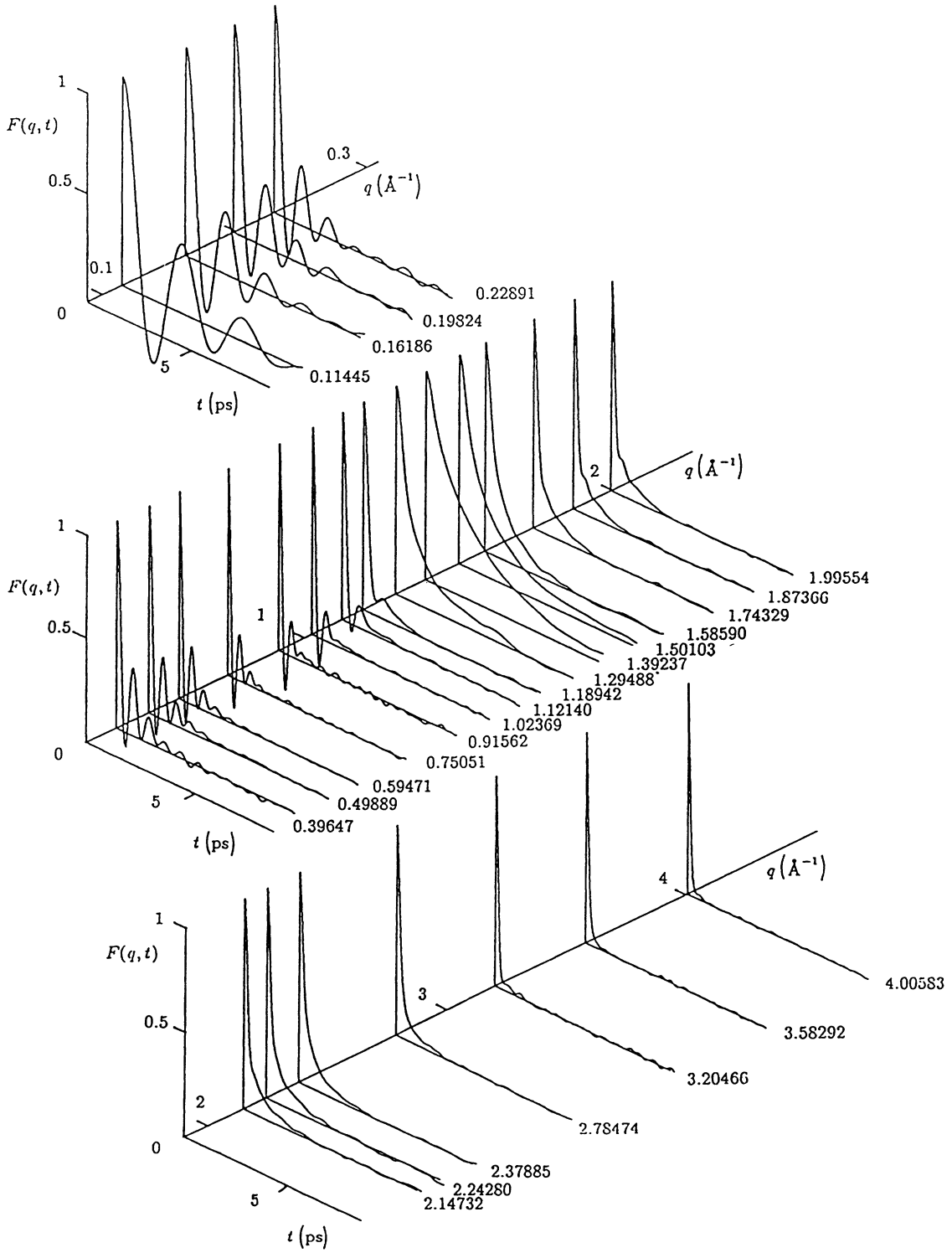

FIG. 9. Normalized intermediate scattering function $F_N(q,t)$ as defined in Fig. 8 for the whole q range investigated. Note the different scales in the q direction; the respective q values are indicated. All results are from the 1372-particle system, except for the four largest q's, which stem from the 256-particle system.

small q's. Balucani and Vallauri [15] also found in the above-mentioned study that a two-time relaxation ansatz is absolutely necessary to describe the decay mechanism in an adequate way. Their model is based on a more sophisticated ansatz (namely, on a MC theory [44]) than our simple phenomenologically derived expression (44). However, they have to make several simplifications in order to practically use their complex expression. In the end, we think that the two models do not differ too much and we both end up with the conclusion that two relaxation times *are in fact* necessary for the MF of $S(q,\omega)$. Expression (40) turns out to be very suitable to fit the computer data over a large q range; we have therefore used this model well *beyond* the hydrodynamic regime, as

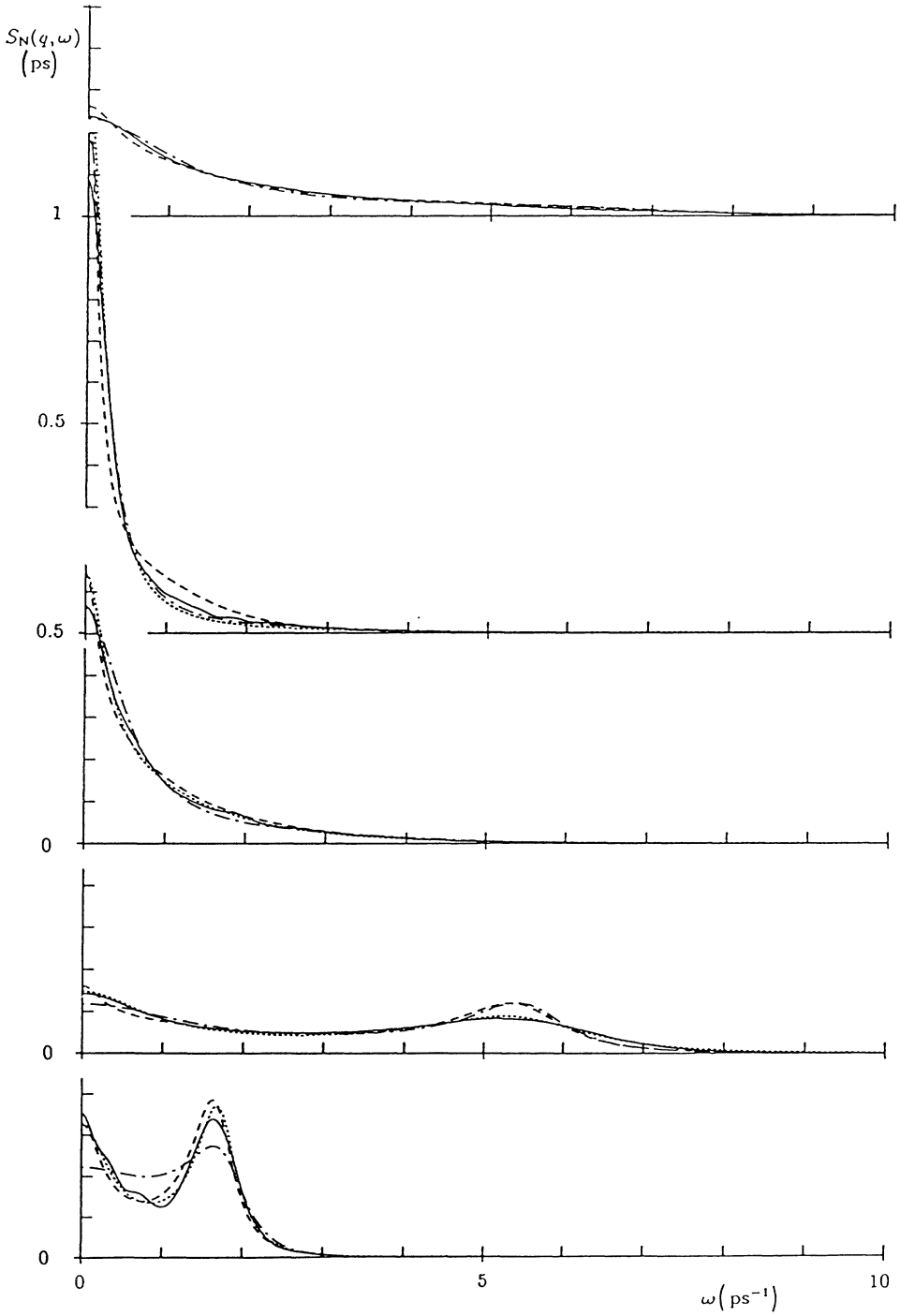

FIG. 10. Comparison of the different methods of FT's of $F(q,t)$ to $S(q,\omega)$ for several q-vectors (from top to bottom: 1.743 29, 1.392 37, 1.294 88, 0.594 71, and 0.161 86 Å^{-1}): full line, (37); broken line, MF-3 ansatz (43)–(46), (33); dashed-dotted line, MF-1 ansatz; and dotted line, HF (40).

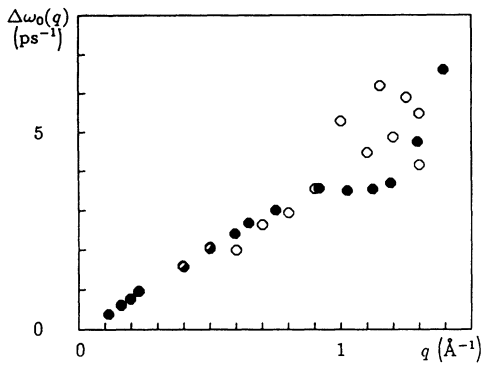

FIG. 11. Full width at half maximum $\Delta\omega_0(q)$ of the inelastic peak in $S(q,\omega)$: ●, theoretical results (obtained from the HF parameters); ○, experimental results [1]; at half-filled circles theoretical and experimental results coincide.

long as the obtained parameters have physical significance; comparison with other FT's (Fig. 10) justifies this. In fact, we used this expression up to $q \sim 1.3$ Å^{-1}, where the velocity of sound becomes negative. Bodensteiner *et al.* [1] have used the same model to fit their experimental data: in Fig. 11 we have depicted both theoretical and experimental values for the full width at half maximum of the inelastic peak $\Delta\omega_0$ (the theoretical values are taken from the HF parameters); agreement up to ~ 1 Å^{-1} is very good, the large scattering of the experimental values beyond this q is due to difficulties in resolving the inelastic peak of the experimental data [45]. The HF- and MF-fitting parameters $\gamma(q)$, $\Gamma(q)$, $D_T(q)$, c_s and $\tau_l(q)$ are depicted in Figs. 12 and 13. The influence of the system size is in general not too large. In Sec. IV C we will discuss possibilities of how to recover the true physical quantities (γ, Γ, D_T, and c_s).

$S_N(q,\omega)=S(q,\omega)/S(q)$ has been compared to the experimental results of Bodensteiner *et al.* [1] over a large q range. This comparison is presented in Fig. 14: agreement with experiment is for intermediate and large q's not only qualitatively but also quantitatively very good. Only for q values smaller than ~ 1 A^{-1} discrepancies in value (*not* in shape) occur for small ω's which may partly be due to small differences in $S(q)$: this quantity, being rather small in this region, is affected with a rather large error and might therefore cause large differences due to the normalization prescription; however, the qualitative agreement is still maintained. The sound mode, which may be traced up to ~ 1.2 Å^{-1}, is reproduced with astonishingly high accuracy. The dispersion relation $\omega_l^m(q)$ is shown both for the theoretical and experimental results in Fig. 15: agreement with experiment is very good. In the same figure we present the phase velocity $c_l(q)$ of the propagating sound modes and finally, in the bottom panel several velocities: the symbols represent $c_l(q)$ and $c_B(q)$ (defined above), the curves depict $c_0(q)=v_0\sqrt{\gamma/S(q)}$ (assuming an experimental value of 1.1 for γ) and the high-frequency sound speed $c_\infty(q)=\sqrt{(1/\rho M)[\frac{4}{3}G_\infty(q)+K_\infty(q)]}$. As in experiment [1] we find for $\omega_l^m(q)$ an anomalous positive dispersion, i.e., an

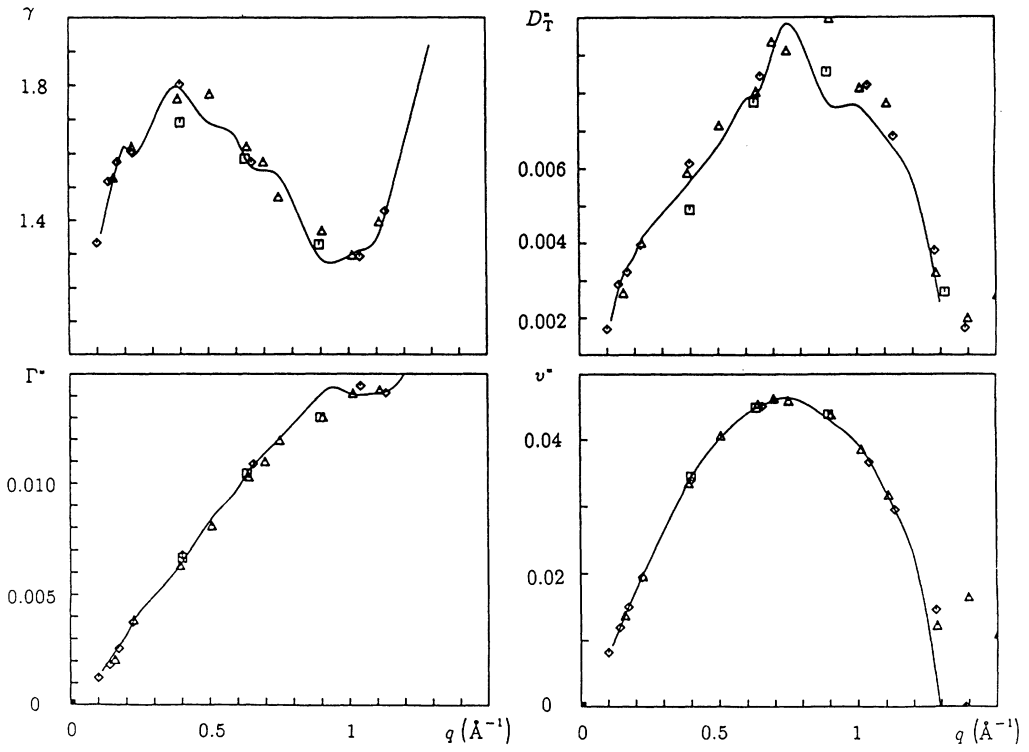

FIG. 12. q dependence of the HF parameters for $S(q,\omega)$ [cf. (40)]. Symbols as in Fig. 3. The following reduced units are used: $\Gamma^*=\Gamma q^2\Delta t$, $D_T^*=D_T q^2\Delta t$, $v^*=c_s q\Delta t$; $\Delta t=8\times10^{-15}$ s.

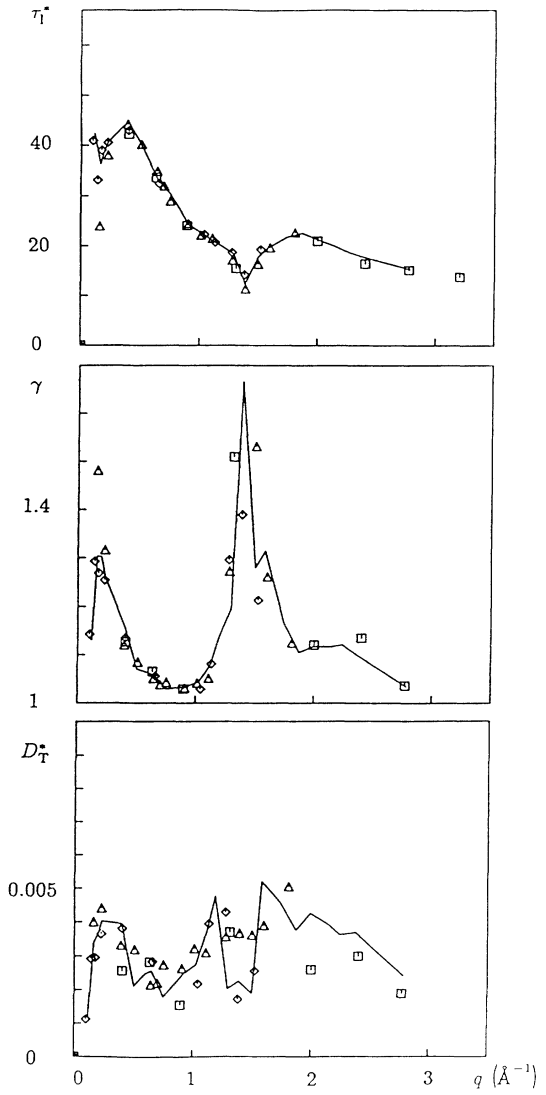

FIG. 13. q dependence of the three MF-fitting parameters of $S(q,\omega)$ [cf. (43)–(46)]. Symbols as in Fig. 12. The following reduced units are used: $\tau_l^* = \tau_l/\Delta t$, $D_T^* = D_T q^2 \Delta t$: $\Delta t = 8 \times 10^{-15}$ s.

enhancement over the linear dispersion. This is nicely seen especially from the second panel where we find a deviation of $c_l(q)$ from a horizontal line (which would correspond to a *linear* dispersion). the bottom panel substantiates what Bodensteiner *et al.* [1] assume to be the reason for the positive dispersion: if shear modes are present—and this is obviously the case both in theory and experiment—then the dispersion skips over from $\omega_l^m(q) \sim c_l(q)q$ to $\omega_l^m(q) \sim c_\infty(q)q$. And in fact $c_\infty(q)$ turns out to be an upper limit to our dispersion curve, as shown in Fig. 15. The theoretical and experimental value for $c_\infty(0)$ differ quite strongly: 1356.2 ms^{-1} (theor.) versus 1109 ms^{-1} (expt.); a direct comparison is, however, not legal, since the experimental value is calculated via a simple model [46] [assuming a model $g(r)$], whereas the theoretical one is directly evaluated from $g(r)$ and $\Phi(r)$ via (35). In order to quantify the positivity of the dispersion relation we use an expression provided by MC theory, which predicts the following small-q behavior of $\omega_B(q)$ [47] (and was substantiated for liquid Ar [48]):

$$\omega_B(q) \sim c_s q + \alpha_s q^{5/2} + O(q^{11/4}) . \tag{54}$$

This expression allows us to determine the *theoretical* value of c_s; α_s is a direct measure of the degree of positivity of $\omega_B(q)$. For these calculations we used $S(q,\omega)$ determined by two different methods [FT via (37) and via the MF model (45)]; results for c_s and α_s are compiled in Table IV.

Experimentalists have assumed [1] that there is evidence for propagating sound modes for q's beyond q_p; we regret to say that computer experiments cannot give a definite answer (only a slight shoulder for 1.6 Å$^{-1} \leq q \leq 1.9$ Å^{-1} is visible in our results). From our data, no evidence could be found for such a mode: neither from studying $S(q,\omega)$ obtained via (37) on a very fine ω grid nor from the analytic expression for the MF-3 model (45). A final decision, however, if theoretical methods are able to predict or to reproduce propagating modes beyond q_p can only be given via MC theory (and will be presented elsewhere): such modes have already been found for liquid Ar [49], even though a distinct peak was not "visible" from the $S(q,\omega)$ curves ["the absence of distinct peaks in $S(q,\omega)$ does not imply the absence of sound modes"].

Although the transverse current CF $C_t(q,t)$ is not accessible from experiment, MD results allow their determination via (30); sampling was done in the same way as for $F(q,t)$. $C_t(q,t)$ has been interpreted in terms of a HF (39) and two MF models [a one-parameter and a three-parameter expression (49)]. The first model gives very poor results (not displayed); this is not surprising, since (39) is an exponentially decaying function in t, whereas computer data oscillate in time. The HF parameter ν as a function of q is depicted in Fig. 16. The quality of the MF models depends strongly on the value of q. For small q's (up to $\sim$0.6 Å^{-1}) the MF-3 is superior to the MF-1; however, as we increase q, (i) the mixing parameter α_t tends to 0 (in fact $\alpha_t < 10^{-3}$ for $q > 1$ Å^{-1}), (ii) the smaller relaxation time (e.g., τ_{1t}) tends to the MF-1 parameter τ_t, and (iii) although τ_{2t} reaches extremely high values, the second decay mechanism loses its significance due to the vanishing prefactor. The MF parameters $\tau_t(q)$ [$\tau_{1t}(q)$, $\tau_{2t}(q)$, and α_t] are shown in Fig. 17 and depict nicely how the MF-3 model merges into the MF-1 expression at $q \sim 0.6$–1 Å^{-1}. We want to point out that the onset of this fact is different from our previous communication [2] where we claimed it to be at the onset of the main peak of $S(q)$ ($\sim$1.2 Å^{-1}). This difference originates from the fact that we have used an improved procedure [as described above for $F_s(q,t)$] to fit the raw computer data. Our findings are in agreement with those of Balucani and co-workers for liquid Rb [15] and in contrast to the data for LJ systems (Levesque, Verlet, and Kurkijärvi [5]), where the authors claim that a two-parameter relaxation

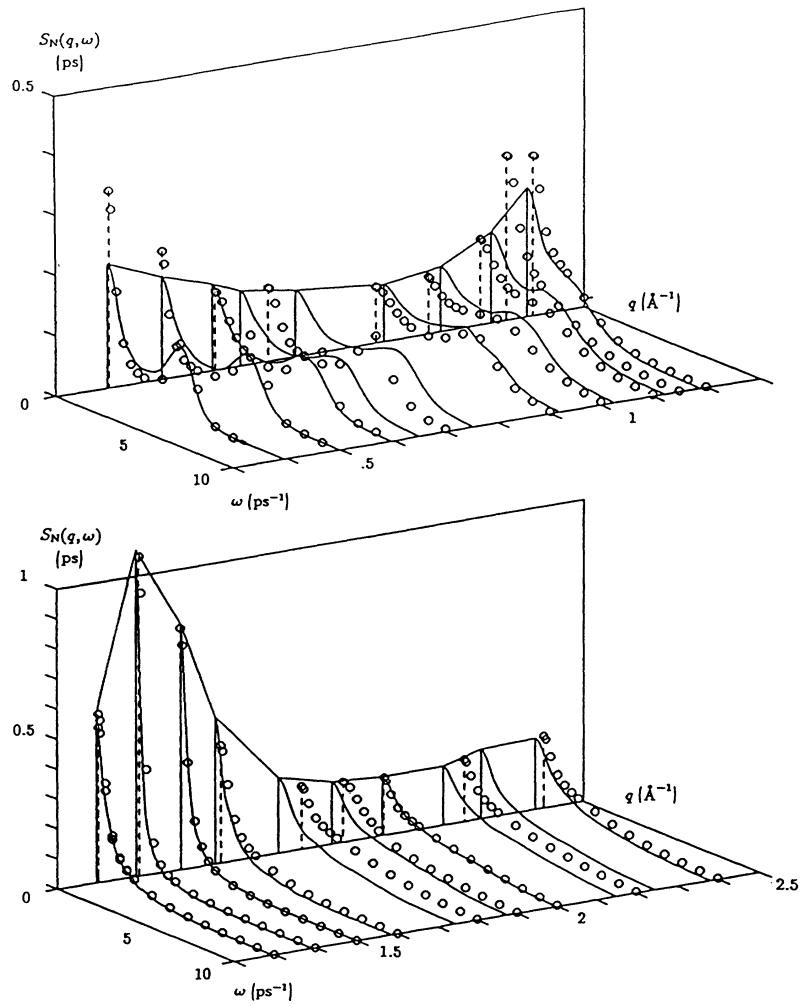

FIG. 14. Normalized dynamic structure factor $S_N(q,\omega)=S(q,\omega)/S(q)$ as obtained from MD [via (37), $N=1372$] and from experiment [1]. Full vertical lines indicate q values of theoretical results, broken vertical lines those of experimental data. The exact q values may be seen from Table II.

ansatz is definitely superior to a one-parameter ansatz. This might indicate that relaxation processes in LJ systems are of a different nature than in liquid metals. In the region where two relaxation processes can be observed (up to ~ 0.6 Å^{-1}), we find that the relaxation times differ by at least one order of magnitude, which means that the decay of the transverse modes depends on two mechanisms: a fast ("binary") and a slow ("collective") one [15,16]. It is clearly seen that for q's up to $\sim 0.6-1$ Å^{-1} both processes contribute to the memory; however, as we reach this q region, the slow relaxation process vanishes completely, i.e., the decay of the transverse modes is entirely supported by the fast "binary" process.

$C_t(q,\omega)$ is depicted in Fig. 18 for the q values of the $N=1372$ ensemble. For all curves a maximum for $\omega>0$ is visible: the position of this maximum determines the dispersion relation $\omega_t^m(q)$ of the transverse modes (Fig. 19). Already up to ~ 1980 it was found that LJ systems and liquid metals show a completely different behavior concerning their ability to support longitudinal and transverse modes: in LJ systems [5] longitudinal modes exist up to $2\pi/6a$ and transverse modes exist from $2\pi/7a$ onwards, where a is the nearest-neighbor distance. In liquid metals [12] longitudinal modes exist up to $2\pi/1.4a$ whereas transverse modes can be supported already from $2\pi/14a$ onwards, i.e., the regions where both modes are observed do overlap. In our case, the q-vector from where shear waves are supported (q_t) is smaller than the

TABLE IV. Theoretical value of the adiabatic sound velocity c_s (in m s^{-1}) and α_s (in 10^{-13}m$^{5/2}$s^{-1}) as obtained via MC theory [cf. text and (54)] from the theoretical dispersion relation for $S(q,\omega)$: (a) from a MF fit to $S(q,\omega)$ and (b) from $S(q,\omega)$ via (37). LSQ is the least-square sum taken over 5 data points.

	(a)	(b)
c_s	1010.7	1032.5
α_s	1.26	0.54
LSQ	0.089	0.0216

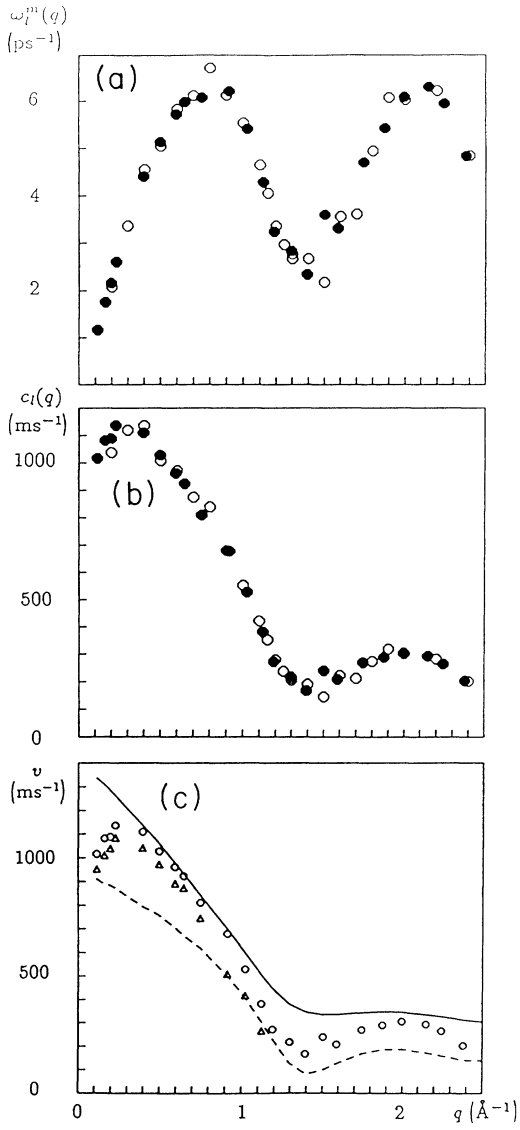

FIG. 15. (a) Dispersion relation of the collective modes $\omega_t^m(q)$: theoretical values (●) in comparison with experimental data [1] (○); (b) phase velocity of the propagating modes $c_l(q)=\omega_l^m(q)/q$ [symbols as in (a)]; (c) different velocities as functions of q: $c_l(q)$, ○; $c_B(q)$, △ (both defined in the text); $c_\infty(q)$ (full line); and $c_0(q)$ (broken line).

smallest q accessible in our experiment; assuming a linear dispersion $\omega_t^m(q)\sim c_t(q-q_t)$ in the vicinity of q_t we obtain (from a linear least-square fit up to $q=0.6$ Å^{-1}) from our results the following values: $c_t=644\text{ms}^{-1}$ and $q_t=0.0732$ Å^{-1}.

We would like to take this occasion to compare our results with data obtained for liquid Rb near the melting point and in the supercooled state by Mountain [51]. Since we know that for the liquid alkali metals near the melting point the static structure scales with $\sim\rho^{-1/3}$ we introduce as a natural length scale the Wigner-Seitz radius $a_{\text{WS}}=(3/4\pi\rho)^{1/3}$. Although the potential used by Mountain [52] is different from ours, both concerning

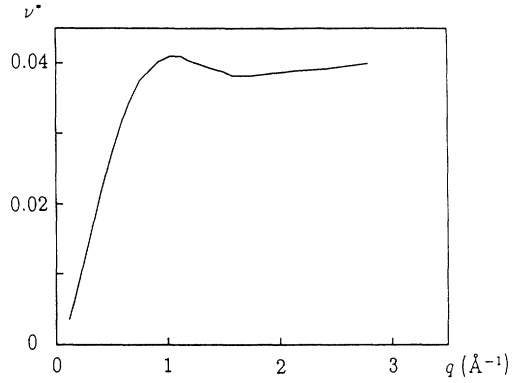

FIG. 16. q dependence of the HF parameter $\nu^*(q)=\nu q^2\Delta t$ of $C_t(q,t)$ [cf. (39)] for $N=1372$; $\Delta t=8\times10^{-15}$ s.

range and depth (cf. Table V) we find an astonishingly good agreement for q_t ($q_t a_{\text{WS}}^{\text{Cs}}=0.224$ versus $q_t a_{\text{WS}}^{\text{Rb}}=0.224$). Perhaps this excellent agreement is fortuitous; only an extensive investigation on the dynamical structure of the liquid alkali metals near the melting point might give a more definite answer. However, in any case this finding may indicate that obviously the shape of the potential (which is for both cases similar) is more important for dynamic properties than the position and the range of the attractive part of the interaction; this would also substantiate the conjecture about the different behavior of liquid metals and LJ: LJ potentials have a strongly anharmonic attractive potential.

C. Elastic and thermodynamic properties

The parameters of the different HF and MF models for the dynamic CF's are generalized, q-dependent elastic and thermodynamic constants. In principle, the physical values are obtained by extrapolating towards $q=0$. However, it turns out that from the numerical point of view this task is a rather tricky one and by no means so

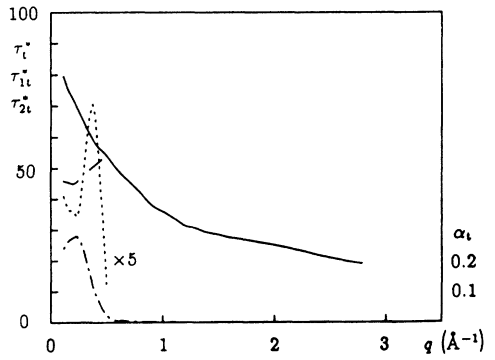

FIG. 17. q dependence of the MF-1 (τ_t) and the MF-3 MF-fitting parameter(s) ($\tau_{1t}^*,\tau_{2t}^*,\alpha_t$) of $C_t(q,t)$ (48) and (49) for $N=1372$. The different τ_t^*'s are in units of $\Delta t=8\times10^{-15}$ s. Symbols: full line, τ_t^*; broken line, τ_{1t}^*; dotted line, τ_{2t}^*; and dashed-dotted line, α_t.

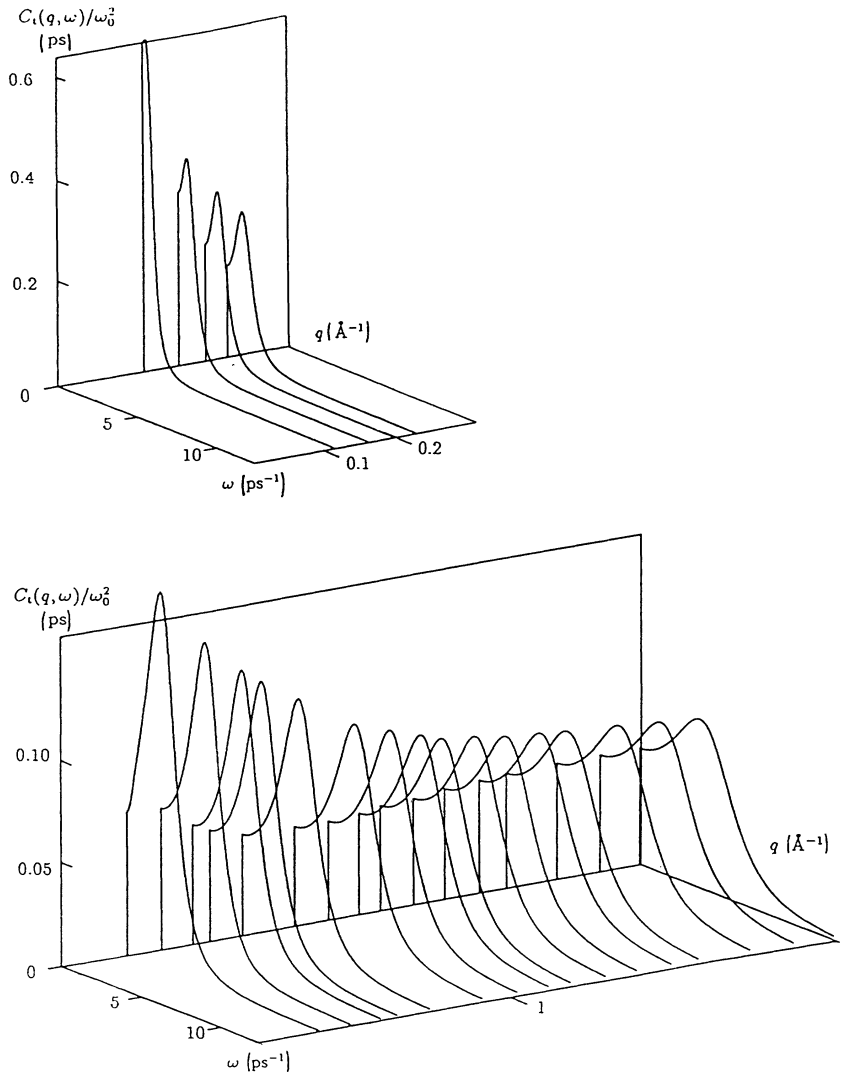

FIG. 18. Spectrum of the transverse current CF $C_t(q,\omega)$ as a function of q and ω for the q-vectors of the $N=1372$ system. Note the different scales in the q direction.

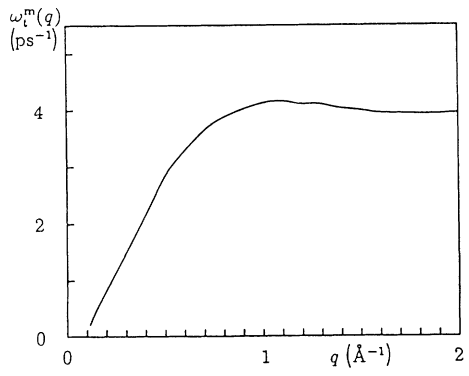

FIG. 19. Transverse dispersion relation $\omega_t^m(q)$ as obtained from the MF-3 model (49) as a function of Q ($N=1372$ results).

trivial as it is usually presented in the literature. This holds especially for the HF case, where the region over which one has to *inter*polate is of about the same size as the region over which one has to *extra*polate towards $q=0$: since these parameters are—due to statistical errors in the CF's—in general not very smooth functions of

TABLE V. Characteristic quantities of the potentials used in this study and of the interaction proposed by Price, Singwi, and Tosi [52] and used in Mountain's study [51] on Rb. $a_{WS}=(3/4\pi\rho)^{1/3}$ is the Wigner-Seitz radius. r_I, r_{II}, and r_{III} are the first zero, the position of the first minimum, and the second zero of the potentials.

	r_I/a_{WS}	r_{II}/a_{WS}	r_{III}/a_{WS}	$\beta\Phi(r_{II}/a_{WS})$
Rb	1.56	1.81	2.56	1.26
Cs	1.49	1.74	2.34	1.81

q, the values obtained for $q=0$ (i.e., the true physical values) depend rather on the number of points involved and/or on the assumed shape of the interpolating and extrapolating function. In the beginning we have used both interpolating functions (polynomial and rational interpolants [53]) and least-square fits (linear and quadratic function shapes). The interpolating functions had to be discarded due to the fact that an increasing number of points involved increases the number of wiggles of these functions and therefore make the value at $q=0$ rather uncertain. So we are left with the least-square fits. In order to make transparent to the reader in which way our results were obtained we use the following notation: L-n stands for a linear least-square fit and Q-n for a quadratic least-square fit, where n is the number of points involved. We found that in general 4 points for the linear fit and 6 points for the quadratic fit are a reasonable number of points.

Table VI contains (i) all those elastic and thermodynamic quantities which may in principle be extracted from the models used here, (ii) the respective experimental value, (iii) from what expression they may be determined, and (iv) if they indeed may be extracted from the raw computer data in a proper way.

The diffusion constant D may be determined in several ways: Table VII contains these different values for D in comparison with the experimental value [1,25]. The theoretical data are—except for method (f)—in reasonably good agreement with experiment. The poor value obtained from the MF fit to $\Psi(t)$ has already been discussed. For D_T we obtain (all values in $10^{-7}\mathrm{m^2\,s^{-1}}$) the following: HF (11): 2.77 (L-4), 3.01 (Q-6); MF-3 (44), (45): 3.04 (L-4), 3.27 (Q-6); although comparison with the experimental value of 3.0 [25] seems to be very satisfying, we have to admit that this agreement is probably due to a fortuitous cancellation of contributions, as will be discussed later. Concerning γ, the ratio of the specific heats, we obtain the following values: HF (40): 1.15 (L-4), 0.95 (Q-6); MF-3 (44), (45): 1.12 (L-4), 1.18 (Q-6), which compare favorably well with the experimental value of 1.1. As already stated above, agreement for $\Gamma(q)$ using both for the theoretical and experimental results a HF model is very good over a large q range. Consequently we find for $\Gamma=\Gamma(0)$ a relatively good agreement [theor.: 1.01 (L-4), 1.10 (Q-6); expt.: 0.83; values in $10^{-7}\mathrm{m^2\,s^{-1}}$]. Results for the adiabatic velocity of sound c_s have already been discussed and are compiled in Table IV. The specific heat C_v has been determined via the temperature

TABLE VI. Thermodynamic and elastic properties which may be extracted from the different models of CF's applied to the computer data (HF = hydrodynamic fit, MF-n=memory-function ansatz with n parameters, and MC=mode-coupling theory) along with their experimental values. "Yes" or "no" in the last column indicates if the limit q towards 0 may be performed in a numerically proper and safe way.

Quantity	Experimental value	Model	Equation	
D	2.35×10^{-9} $\mathrm{m^2\,s^{-1}}$ [25]	HF to $F_s(q,t)$	(11)	yes
		MF-1 to $F_s(q,t)$	(17), (18)	yes
		MF to $\Psi(t)$	(24), (25)	yes
		time integral of $\Psi(t)$	(26)	yes
		Gaussian model for $F_s(q,t)$	(28)	yes
		mean-square displacement	(52)	yes
		MC	(53)	yes
D_T	3.0×10^{-7} $\mathrm{m^2\,s^{-1}}$ [25]	HF to $F(q,t)$	(38), (40)	yes
		MF-3 to $F(q,t)$	(44), (45)	yes
γ	1.102 [25]	HF to $F(q,t)$	(38), (40)	yes
		MF-3 to $F(q,t)$	(44), (45)	yes
Γ	8.3×10^{-7} $\mathrm{m^2\,s^{-1}}$ [25]	HF to $F(q,t)$	(38), (40)	yes
c_s	965 $\mathrm{m\,s^{-1}}$ [25]	HF to $F(q,t)$	(38), (40)	yes
		MC to $\omega_l^m(q)$	(54)	yes
C_v	0.214 $\mathrm{J\,g\,K^{-1}}$ [25]	temperature variation	(51)	yes
$\eta=\rho M\nu$	0.7×10^{-3} Pa s [26]	HF to $C_t(q,t)$	(41)	yes
		MF-1 to $C_t(q,t)$	(49), (50)	yes
		MF-3 to $C_t(q,t)$	(49), (50)	yes
		MC to $S_s(q,\omega)$	(53)	yes
η_l	2.973×10^{-3} Pa s [26]	Mf-3 to $F(q,t)$	(44), (45), (47)	no
		HF to $S(q,\omega)$	(42)	no

TABLE VII. Diffusion constant D as obtained from different methods (all values in 10^{-9} m^2 s^{-1}): (a) experimental value [1,25]; (b) from MF fit to $S_s(q,\omega)$ (17), (18), (Q-10); (c) from the HF to $S_s(q,\omega)$ (11) (Q-10); (d) the long-time behavior of the Gaussian function $\rho_1(t)$ (cf. text); (e) from time integration of $\Psi(t)$ (26); (f) from MF fit to $\Psi(t)$ (24); (g) from the mean-square displacement (52); (h) from MC to $\omega_s^{1/2}(q)$ and $S_s(q,0)$ (53) (averaged).

(a)	(b)	(c)	(d)	(e)	(f)	(g)	(h)
2.35	2.825	2.204	2.109±0.177	1.8965	3.045 31	1.974±0.0021	2.41±0.015

variation during the MD run (51). We find a value of 0.223 J g K^{-1} versus the experimental result of 0.214 J g K^{-1}. The data for η (and hence for ν) are compiled in Table VIII. Similar to D the agreement with the experimental value is satisfactory except for method (e). The longitudinal viscosity $\eta_l = \frac{4}{3}\eta + \eta_B$ has been determined via two different routes: using the MF-3 values for $S(q,\omega)$ via (47) we obtain 5.36×10^{-4} Pa s, which is nearly one order of magnitude smaller than the experimental value of 2.973×10^{-3} Pa s; the results obtained from the HF fit to $S(q,\omega)$ via (42) are at least in the right order of magnitude [3.625×10^{-3} Pa s (L-4) and 4.06×10^{-3} Pa s (Q-6)]; they still differ quite strongly from the experimental value. First of all (though to a smaller extent) this disagreement may be attributed to numerical reasons: (i) in the MF case the value of η_l depends in a very sensitive way on $S(0)$ [cf. (47)], (ii) in the HF case η_l is calculated from three extrapolated quantities [cf. (42)], where each is affected by statistical errors. However, the main source of the error stems from the fact that we have neglected the contributions from the electronic degrees of freedom; this holds not only for η_l but also for D_T. To include theories of how to treat the electronic contributions properly would clearly pass beyond the frame of this paper. We would only like to point out that this problem is discussed widely by Shimoji [54]: he demonstrates on several examples that for these quantities the electronic contributions are substantial.

For those elastic properties where agreement of experimental and theoretical data (obtained by extrapolating generalized q-dependent parameters towards $q=0$) is not satisfactory, there exists a further possibility for their determination: via different Green-Dubo relations (compiled, e.g., in Table 8.1 of Hansen and McDonald [21]), several of these quantities may be expressed as time integrals over different CF's [e.g., (26) is such a relation between D and $\Psi(t)$]; these CF's are in general more complicated than the CF's presented here. Nevertheless their evaluation in a MD run follows the same principles as outlined here; several applications with satisfactory results exist [7,50,55].

TABLE VIII. Shear viscosity η as obtained from different methods (all values in 10^{-3} Pa s): (a) experimental value [26]; (b) from HF fit to $C_t(q,t)$ (41); (c) from MF-1 fit to $C_t(q,t)$ (49), (50); (d) from MF-3 fit to $C_t(q,t)$ (49), (50); (e) from MC to $\omega_s^{1/2}(q)$ and $S_s(q,\omega)$ (53) (averaged).

(a)	(b)	(c)	(d)	(e)
0.7	0.781 (L-4) 0.816 (Q-6)	0.752 (L-4) 0.777 (Q-6)	0.714 (L-4) 0.903 (Q-6)	0.44±0.124 (L-8)

V. CONCLUSIONS

In this paper we have reported on a direct comparison between theoretical and experimental results of the dynamic properties of liquid cesium just above the melting point; while the experimental data were obtained by *neutron-scattering*, our experiment was done on a *computer* in a MD study. Agreement between theory and experiment, both for the dynamic structure factor and the dispersion relation, is very good; the latter shows also in the computer experiment a positive dispersion, i.e., an enhancement over the linear dispersion (adiabatic sound speed). As in the experimental results we find that the high-frequency sound speed c_∞ turns out to be an upper limit of the dispersion, which means that shear waves are probably responsible for this anomaly. Sufficient evidence for propagating sound modes for q's beyond the main peak of the static structure factor could not be found. However, further analysis of our results in terms of MC theory might reveal their existence. For the damping of the inelastic peak in $S(q,\omega)$ we find very good agreement with experiment. We have also determined other CF's which are not accessible via experiment, either due to the small incoherent neutron-scattering cross section of Cs or due to principal reasons, i.e., the single-particle CF's and the transverse current CF's. Concerning $S_s(q,\omega)$ the small-q behavior for the ($\omega=0$) value and the full width at half maximum reproduce very accurately the expressions predicted by MC theory. The VACF $\Psi(t)$ shows a strongly oscillating behavior, i.e., the cage effect is dominant, where the particles are enclosed in small cages of the liquid where they collide frequently and thus lose memory of their initial velocity very quickly. The memory of the transverse current CF turns out to be built up for small q's from two principal processes, a "binary" fast one and a "collective" slow one (the relaxation time of the latter being by one or two orders of magnitude larger); however, from $\sim 0.6-1$ Å^{-1} onwards, the collective contribution is completely extinguished, i.e., we are left with a one-relaxation time model.

All CF's have been fitted to several HF and MF models, involving generalized, q-dependent thermodynamic and elastic quantities as parameters. If statistics allows a safe extrapolation of these quantities towards $q=0$, the

true physical values could be recovered. Then, agreement with the experimental values was in general very satisfactory (i.e., differences of 10–15 % are observed).

ACKNOWLEDGMENTS

The authors would like to thank Professor J. Hafner (Wien), Professor Y. Hiwatari (Kanazawa), Professor C. Hoheisel (Bochum), Professor D. Levesque, and Professor J.-J. Weis (both Paris) for many interesting and stimulating discussions and useful hints. Special thanks to Dr. C. Morkel (München) for providing detailed experimental data [1], for many helpful discussions and for bringing Refs. [30,31] to our attention. This work was supported by the Österreichische Forschungsfonds under Project No. P7618-TEC.

---

*Present address: Computing and Information Systems Center, Tokai Research Establishment, JAERI, Tokai, Naka, Ibaraki 319-11, Japan.

[1] T. Bodensteiner, Ph.D. thesis, Technische Universität München (1990); C. Morkel and T. Bodensteiner, J. Phys. (Cond. Matter) **2**, SA 251 (1990); T. Bodensteiner, C. Morkel, W. Gläser, and B. Dorner, Phys. Rev. A **45**, 5709 (1992).

[2] S. Kambayashi and G. Kahl, Europhys. Lett. **18**, 421 (1992).

[3] A. Rahman, Phys. Rev. **136**, A405 (1964).

[4] D. Levesque and L. Verlet, Phys. Rev. A **2**, 2514 (1970).

[5] D. Levesque, L. Verlet, and J. Kurkijärvi, Phys. Rev. A **7**, 1690 (1973).

[6] R. Vogelsang and C. Hoheisel, Mol. Phys. **53**, 1255 (1984); M. Schoen and C. Hoheisel, *ibid.* **58**, 181 (1986).

[7] C. Hoheisel, R. Vogelsang, and M. Schoen, J. Chem. Phys. **87**, 7195 (1987).

[8] M. Schoen, R. Vogelsang, and C. Hoheisel, Mol. Phys. **57**, 445 (1986).

[9] J.-P. Boon and S. Yip, *Molecular Hydrodynamics* (McGraw-Hill, New York, 1980).

[10] A. Rahman, Phys. Rev. A **4**, 1667 (1974); Phys. Rev. Lett. **32**, 52 (1974).

[11] J. R. D. Copley and J. M. Rowe, Phys. Rev. A **4**, 1656 (1974); J. R. D. Rowe and J. M. Copley, Phys. Rev. Lett. **32**, 49 (1974).

[12] G. Jacucci and I. R. McDonald, Mol. Phys. **39**, 515 (1980).

[13] S. W. Haan, R. D. Mountain, C. S. Hsu, and A. Rahman, Phys. Rev. A **22**, 767 (1980).

[14] J. Hafner and V. Heine, J. Phys. F **13**, 2479 (1983).

[15] U. Balucani and R. Vallauri, Phys. Rev. A **40**, 2796 (1989).

[16] U. Balucani, R. Vallauri, and T. Gaskell, Phys. Rev. A **35**, 4263 (1987).

[17] M. Dzugutov, K.-E. Larsson, and I. Ebbsjö, Phys. Rev. A **38**, 3609 (1988); M. Dzugutov and U. Dahlborg, *ibid.* **40**, 4103 (1989).

[18] P. H. K. deJong, P. Verkerk, S. Ahda, and L. A. deGraaf, in *Recent Development in the Physics of Fluids,* edited by W. S. Howells and A. K. Soper (Hilger, Bristol, 1992), p. F223.

[19] W. Mountfrooy, I. de Schepper, J. Bosse, W. Gläser, and C. Morkel, Phys. Rev. A **33**, 1405 (1986); C. Morkel, C. Gronemeyer, W. Gläser, and J. Bosse, Phys. Rev. Lett. **18**, 1873 (1987).

[20] C. Pilgrim, R. Winter, F. Hensel, C. Morkel, and W. Gläser, in *Recent Development in the Physics of Fluids,* edited by W. S. Howells and A. K. Soper (Hilger, Bristol, 1992), p. F181; C. Pilgrim, R. Winter, F. Hensel, C. Morkel, and W. Gläser (unpublished).

[21] J.-P. Hansen and I. R. McDonald, *Theory of Simple Liquids,* 2nd ed. (Academic, London, 1986).

[22] N. W. Ashcroft, Phys. Lett. **23**, 48 (1966).

[23] S. Ichimaru, Rev. Mod. Phys. **54**, 1027 (1982); S. Ichimaru and K. Utsumi, Phys. Rev. B **24**, 7381 (1981).

[24] G. Kahl and J. Hafner (unpublished).

[25] R. Ohse, *Handbook of Thermodynamic and Transport Properties of Alkali Metals* (Blackwell Scientific, Oxford, 1985).

[26] M. Shimoji and T. Itami, *Atomic Transport in Liquid Metals* (Trans Tech, Aedermannsdorf, Switzerland, 1986).

[27] J. Hafner, *From Hamiltonians to Phase Diagrams* (Springer, Berlin, 1987).

[28] G. Pastore and M. P. Tosi, Physica B **124**, 383 (1984); J. Hafner and G. Kahl, J. Phys. F **14**, 2259 (1984); G. Kahl and J. Hafner, Solid State Commun. **49**, 1125 (1984); G. Kahl and J. Hafner, Z. Phys. B **58**, 2259 (1985); G. Kahl and G. Pastore, Europhys. Lett. **7**, 36 (1988).

[29] J. A. Moriarty, Phys. Rev. B **26**, 1754 (1982).

[30] N. Nücker and U. Buchenau, Phys. Rev. B **31**, 5479 (1985).

[31] J. Mizuki and C. Stassis, Phys. Rev. B **34**, 5890 (1986).

[32] A. Arnold, N. Mauser, and J. Hafner, J. Phys. (Cond. Matter) **1**, 965 (1989).

[33] D. Levesque and W. T. Ashurst, Phys. Rev. Lett. **33**, 977 (1974).

[34] Y. Rosenfeld, D. Levesque, and J.-J. Weis, J. Chem. Phys. **92**, 6818 (1990).

[35] A. Baranyai and D. J. Evans, Phys. Rev. A **40**, 3817 (1989); **42**, 849 (1990).

[36] J.-L. Barrat, J.-P. Hansen, and G. Pastore, Phys. Rev. Lett. **58**, 2075 (1987); Mol. Phys. **63**, 747 (1988); A. D. J. Haymet, S. A. Rice, and W. G. Madden, J. Chem. Phys. **75**, 4696 (1981); I. Nezbeda and G. Kahl, Chem. Phys. Lett. **183**, 337 (1991); B. Bildstein and G. Kahl (unpublished).

[37] J.-P. Hansen and M. L. Klein, Phys. Rev. B **13**, 878 (1976); Y. Hiwatari and H. Miyagawa, J. Non-Cryst. Solids **117/118**. 862 (1990); M. P. Allen and D. J. Tildesley, *Computer Simulation of Liquids* (Oxford Science, Oxford, 1990).

[38] P.-G. de Gennes, Physica **25**, 825 (1959).

[39] P. Verkerk, J. H. Builtjes, and I. M. de Schepper, Phys. Rev. A **31**, 1731 (1985).

[40] G. Kahl and S. Kambayashi (unpublished).

[41] B. J. Alder and T. E. Wainwright, Phys. Rev. A **1**, 18 (1970).

[42] J. R. Dorfman and E. G. D. Cohen, Phys. Rev. A **6**, 776 (1972); I. M. de Schepper and M. H. Ernst, Physica (Amsterdam) **98A**, 189 (1979); J. Bosse, W. Götze, and M. Lücke, Phys. Rev. A **20**, 1603 (1979).

[43] S.-H. Chen and A. Rahman, Mol. Phys. **34**, 1247 (1977).

[44] L. Sjögren, Phys. Rev. A **22**, 2866 (1980).
[45] C. Morkel (private communication).
[46] J. Hubbard and J. L. Beeby, J. Phys. C **2**, 556 (1969).
[47] H. Ernst and J. R. Dorfmann, Physica **61**, 157 (1972); H. Ernst and J. R. Dorfmann, J. Stat. Phys. **12**, 311 (1975).
[48] I. M. de Schepper, P. Verkerk, A. A. van Well, and L. A. de Graaf, Phys. Lett. **104A**, 29 (1984).
[49] I. M. de Schepper, P. Verkerk, A. A. van Well, and L. A. de Graaf, Phys. Rev. Lett. **50**, 974 (1983).
[50] H. Schaink and C. Hoheisel, J. Chem. Phys. **93**, 2754 (1990).
[51] R. D. Mountain, Phys. Rev. A **26**, 2859 (1982).
[52] D. L. Price, K. S. Singwi, and M. P. Tosi, Phys. Rev. B **2**, 2983 (1976).
[53] W. H. Press, B. P. Flannery, S. A. Teukolsky, and W. T. Vetterling, *Numerical Recipes* (Cambridge University Press, Cambridge, 1988).
[54] M. Shimoji, *Liquid Metals* (Academic, London, 1977).
[55] D. Levesque, J.-J. Weis, and J. Vermesse, Phys. Rev. A **37**, 918 (1988); D. Levesque and J.-J. Weis, *ibid.* **37**, 3967 (1988).